

# 1 **A single-column ocean-biogeochemistry model (GOTM-TOPAZ)** 2 **version 1.0**

3 Hyun-Chae Jung<sup>1</sup>, Byung-Kwon Moon<sup>1</sup>, Jieun Wie<sup>1</sup>, Hye-Sun Park<sup>2</sup>, Johan Lee<sup>3</sup>, Young-Hwa Byun<sup>3</sup>

4 <sup>1</sup>Division of Science Education, Institute of Fusion Science, Chonbuk National University, Jeonju 54896, South Korea

5 <sup>2</sup>Cray Korea Inc., Seoul 08511, South Korea

6 <sup>3</sup>National Institute of Meteorological Sciences, Seogwipo 63568, South Korea

7 *Correspondence to:* Byung-Kwon Moon (moonbk@jbnu.ac.kr)

8 **Abstract.** Recently, Earth System Models (ESMs) have begun to consider the marine ecosystem to reduce errors in climate  
9 simulations. However, many models are unable to fully represent the ocean biology-induced climate feedback, which is due  
10 in part to significant bias in the simulated biogeochemical properties. Therefore, we developed the Generic Ocean  
11 Turbulence Model–Tracers of Phytoplankton with Allometric Zooplankton (GOTM-TOPAZ), a single-column ocean  
12 biogeochemistry model that can be used to improve ocean biogeochemical processes in ESMs. This model was developed by  
13 combining the GOTM, a single-column model that can simulate the physical environment of the ocean, and TOPAZ, a  
14 biogeochemical module. Here, the original form of TOPAZ has been modified and modularized to allow easy coupling with  
15 other physical ocean models. To demonstrate interactions between ocean physics and biogeochemical processes, the model  
16 was designed to allow ocean temperature to change due to absorption of visible light by chlorophyll in phytoplankton. We  
17 also added a module to reproduce upwelling and the air-sea gas transfer process for oxygen and carbon dioxide, which are of  
18 particular importance for marine ecosystems. The simulated variables (e.g., chlorophyll, oxygen, nitrogen, phosphorus,  
19 silicon) of GOTM-TOPAZ were evaluated by comparison against observations. The temporal variability of the observed  
20 upper-ocean (0–20 m) chlorophyll is well captured by the GOTM-TOPAZ model with a correlation coefficient of 0.51. The  
21 surface correlation coefficients between the GOTM-TOPAZ oxygen, nitrogen, phosphorus, and silicon are 0.47, 0.30, 0.16,  
22 and 0.19, respectively. We compared the GOTM-TOPAZ simulations with those from MOM-TOPAZ and found that  
23 GOTM-TOPAZ showed relatively lower correlations, which is most likely due to the limitations of the single-column model.  
24 **Results also indicate that source/sink terms may contribute to the biases in the surface layer (< 60 m), while initial values are**  
25 **important for realistic simulations in the deep sea (> 250 m).** Despite this limitation, we argue that our GOTM-TOPAZ  
26 model is a good starting point for further investigation of key biogeochemical processes and is also useful to couple complex  
27 biogeochemical processes with various oceanic global circulation models.

28

## 29 **1 Introduction**

30 Over several decades, climate researchers have accumulated significant knowledge on atmosphere-land-ocean feedback  
31 processes through various studies related to climate systems (Friedlingstein et al., 2006; Soden and Held, 2006; Dirmeyer et  
32 al., 2012; Randerson et al., 2015). With the advancement of coupled modeling techniques and an exponential increase in the  
33 number of computer resources available, climate research institutions worldwide began competing to develop earth system  
34 models (ESMs) (Dunne et al., 2012a; Dunne et al., 2012b; Jones and Sellar, 2015; Sokolov et al., 2018). ESMs are often  
35 coupled with biogeochemistry models that consider the atmosphere–ocean carbon cycle and ocean ecosystem cycles (Dunne  
36 et al. 2012b; Yool et al., 2013; Azhar et al., 2014; Stock et al., 2014; Aumont et al., 2015). Recently, reproductions of ocean  
37 ecosystems in ESMs have become very precise with the addition of physiological details, such as light or nutrient  
38 acclimation, and the division of various phytoplankton and zooplankton into functional groups (Hense et al., 2017).

39 The following processes are generally considered the most important in ocean biogeochemistry models: the ocean  
40 ecosystem cycle, including phytoplankton and zooplankton; the biogeochemical carbon cycle; and the biogeochemical cycle  
41 of key nutrients (P, N, Fe, and Si) (Dunne et al., 2012b; Aumont et al., 2015). These three cycles are not independent and  
42 include mutual material exchange through chemical mechanisms. There are still no accurate methodologies with which to  
43 differentiate biogeochemical variables and to represent biogeochemical processes as formulas (Sauerland et al., 2018). In  
44 other words, biogeochemical processes are reproduced in the model via parameterization that adjusts the parameters of a  
45 formula based on observations and some general parameters (e.g., maximum phytoplankton growth rate) that are adjusted  
46 until the model produces reasonable results (Sauerland et al., 2018).

47 Researchers have been using single-column models (SCMs) to control the parameterizations and increase their  
48 understanding of the physical processes in models. Betts and Miller (1986) suggested that SCMs were an effective tool with  
49 which to develop and control the convective scheme of an atmospheric model, while Price et al. (1986) used an ocean SCM  
50 to study the daily cycle of the mixed layer in the Pacific Ocean. An SCM allows for control of physics parameters, alongside  
51 large-scale forcing influences, and, unlike 3D models, it has a low calculation cost. Accordingly, SCMs have been viewed as  
52 essential tools with which to develop and improve numerical models (Lebassi-Habtezion and Caldwell, 2015; Hartung et al.,  
53 2018). SCM-based studies are essential for improving ocean-biogeochemical processes, which are reproduced in climate  
54 models based on column physics (Evans and Garçon, 1997; Burchard et al., 2006; Bruggenman and Bolding, 2014). Even  
55 the latest analyses of the ESMs included in the Coupled Model Intercomparison Project Phase 5 (CMIP5) show high biases  
56 and inter-model diversity in ocean biogeochemical variables (Lim et al., 2017). Therefore, a single-column form of a  
57 biogeochemistry model might be a useful tool to meet the ongoing demand for improvements in biogeochemistry models in  
58 ESMs.

59 The oceanic biogeochemical cycle affects not only the physical environment of the upper ocean but also that of the entire  
60 climate system, and such changes produce feedback that, in turn, alters the ocean ecosystem (Hense et al., 2017; Lim et al.,  
61 2017; Park et al., 2018). Hense et al. (2017) presented the CO<sub>2</sub> cycle, gas and particle cycle, and changes in the physical

62 environment of the upper ocean by chlorophyll as important climate-ocean biogeochemistry feedback loops reproduced in  
 63 ESMs that are currently available. An ESM that reproduces all three of these biological mechanisms does not exist today;  
 64 however, all of these mechanisms need to be properly reproduced in the ESMs to reduce the uncertainty in predicting future  
 65 climate change. This would allow ESMs to change in a fundamentally different way. Furthermore, there are generally time  
 66 constraints in repeated experiments using ocean general circulation models (OGCMs) and biogeochemistry models due to  
 67 their complexity and the heavy calculation required. Consequently, SCMs are crucial for applying and testing new climate-  
 68 ocean-biogeochemistry feedbacks in existing ESMs.

69 In this study, we developed the Generic Ocean Turbulence Model–Tracers of Phytoplankton with Allometric Zooplankton  
 70 (GOTM-TOPAZ), which is a single-column ocean-biogeochemistry model. GOTM is a one-dimensional ocean model that  
 71 focuses on reproducing statistical turbulence closures (see <http://www.gotm.net>); TOPAZ is an ocean-biogeochemistry  
 72 model developed by the Geophysical Fluid Dynamics Laboratory (GFDL) and coupled with the ESM2M and ESM2G  
 73 models (Dunne et al., 2012a; Dunne et al., 2012b). We modularized TOPAZ to apply external physical environmental data  
 74 while modifying it as an SCM. It was then combined with a GOTM utilizing an air-sea gas exchange for CO<sub>2</sub> and O<sub>2</sub> and  
 75 optical feedback from photosynthesis by chlorophyll. A w-advection prescription module that can reproduce upwelling was  
 76 also added to this model. To verify GOTM-TOPAZ, we selected points in the East/Japan Sea off the coast of the Korean  
 77 Peninsula upon which to conduct simulations. The results produced by the model were compared to observed data and  
 78 results from OGCMs to verify its reliability.

79

## 80 **2 The Physical Ocean Model: General Ocean Turbulence Model (GOTM)**

81 In GOTM-TOPAZ, the GOTM version 4.0 is applied to ocean physics. The physical bases of the GOTM are Reynolds-  
 82 averaged Navier–Stokes equations in a rotational coordinate system (Eqs. 1 and 2). Moreover, the temperature and salinity  
 83 equations derived using these methods are given in Eqs. 3 and 4, respectively. GOTM uses one-dimensional potential  
 84 temperature, salinity, and horizontal velocity based on these four equations, as shown below:

85

$$86 \quad \partial_t u - \nu \partial_{zz} u + \partial_z \langle u'w' \rangle = -\frac{1}{\rho_0} \partial_x p + fv \quad (1)$$

$$87 \quad \partial_t v - \nu \partial_{zz} v + \partial_z \langle v'w' \rangle = -\frac{1}{\rho_0} \partial_y p - fu \quad (2)$$

$$88 \quad \partial_t T - \nu' \partial_{zz} T + \partial_z \langle w'T' \rangle = \frac{\partial_z l}{c_p \rho_0} \quad (3)$$

$$89 \quad \partial_t S - \nu'' \partial_{zz} S + \partial_z \langle w'S' \rangle = \tau_R^{-1} (S_R - S). \quad (4)$$

90

91 In Eqs. (1) and (2),  $u$ ,  $v$ , and  $w$  represent the mean velocities in the spatial directions  $x$  (eastward),  $y$  (northward), and  $z$   
 92 (upward), respectively;  $\nu$  represents the molecular diffusivity of momentum;  $\rho_0$  represents a constant reference density;  $p$

93 represents pressure; and  $f$  represents the Coriolis parameter. In Eq. (3), the temperature ( $T$ ) equation,  $v'$  represents the  
 94 molecular diffusivity due to heat;  $c_p$  represents the heat capacity; and  $I$  represents the vertical divergence of short-wave  
 95 radiation. The effect of solar radiation absorbed by seawater is included in this equation; thus, Eq. (3) is closely associated  
 96 with the radiation parameterization method. Moreover, a coupled ocean biogeochemistry model must contain an additional  
 97 short-wave absorption process associated with chlorophyll synthesis distributed throughout the upper-ocean layer (Morel and  
 98 Antoine, 1994; Cloern et al., 1995; Manizza et al., 2005; Litchman et al., 2015; Hense et al., 2017). Based on the  
 99 methodology of Manizza et al. (2005), we applied a visible light absorption process due to chlorophyll synthesis, explained  
 100 in detail in Sect 4.4, to the coupled model. Equation (4) explains the vertical distribution of salinity ( $S$ ). In this equation,  $v''$   
 101 represents the molecular diffusivity of salinity;  $\tau_R$  represents the relaxation time scale; and  $S_R$  represents the observed  
 102 salinity distribution. In other words, the terms on the right side of this equation express the “relaxation” process based on  
 103 observations. Unlike 3D models, SCMs cannot reproduce horizontal advection. Therefore, as salinity is greatly affected by  
 104 horizontal advection, it is necessary to prescribe and supplement the observed value to the simulated value with the terms on  
 105 the right side of Eq. (4) (Burchard et al., 2006). Please see Umlauf and Burchard (2003, 2005), Umlauf et al. (2005), and  
 106 Burchard et al. (2006) for further detailed information on the GOTM.

107

### 108 **3 The Ocean Biogeochemistry Model: Tracers of Phytoplankton with Allometric Zooplankton (TOPAZ)**

109 We chose TOPAZ version 2.0 to couple with the GOTM. TOPAZ simulates the nitrogen, phosphorus, iron, dissolved  
 110 oxygen, and lithogenic material cycles as well as the ocean carbon cycle while also considering zooplankton and  
 111 phytoplankton growth cycles. It divides phytoplankton into small and large groups based on size, including the group of  
 112 nitrogen-fixing diazotrophs. Consequently, TOPAZ handles a total of 30 prognostic and 11 diagnostic tracers. The local  
 113 changes in the tracers simulated in TOPAZ can be explained by the following equation:

114

$$115 \partial_t C = -\nabla \cdot \vec{v}C + \nabla K \nabla C + S_C. \quad (5)$$

116

117 Equation (5) is an advection-diffusion equation for each state variable  $C$  simulated in TOPAZ. In this equation,  $\vec{v}$   
 118 represents the velocity vector calculated in the ocean model,  $K$  represents diffusivity, and  $S_C$  represents the sources minus the  
 119 sinks of  $C$  calculated at each point in the model. TOPAZ is received data from the ocean model in terms of the transport  
 120 tendency of the tracers associated with advection and horizontal diffusion, and it calculates vertical diffusion and source/sink  
 121 terms internally. The biological processes of TOPAZ were reproduced with a focus on phytoplankton growth, nutrient and  
 122 light limitations, the grazing process, and empirical formulas derived from observations. These are followed by the Redfield  
 123 ratio (Redfield et al., 1963), Liebig’s law of the minimum (de Baar, 1994), and size considerations (large organisms feed on

124 smaller ones), which were used to establish the ocean ecosystem model (Dunne et al., 2012b). Please see Dunne et al. (2012b)  
125 for further detailed information on TOPAZ.

126

## 127 **4 The Ocean Biogeochemistry Coupled Model: GOTM-TOPAZ**

128 TOPAZ was initially coupled with Modular Ocean Model 5 (MOM5), an OGCM developed by the GFDL. We separated  
129 TOPAZ from MOM5 and constructed two modules by separating the initialization and main calculation subroutines. This  
130 model was then modified into an SCM while adding interfaces associated with surface flux prescriptions (boundary  
131 conditions) and initial data input.

132 In our new coupled model, the GOTM provided ocean physics calculations for TOPAZ, and TOPAZ relayed optical  
133 feedback from the chlorophyll simulated according to these data to GOTM. A subroutine that calculates the optical feedback  
134 from chlorophyll and another that prescribes the w-advection were added to GOTM-TOPAZ (see Fig. 1 for the flow  
135 diagram). Upwelling that usually occurs along coastal areas due to wind plays a major role in changing the vertical  
136 distribution of zooplankton and phytoplankton by supplying the surface layer with nutrient-rich intermediate water (Krezel et  
137 al., 2005; Lips and Lips, 2010; Shin et al., 2017). We connected the w-advection module in GOTM to TOPAZ so that the  
138 upwelling was reproduced in TOPAZ.

139

### 140 **4.1 Initial Conditions**

141 The initial data needed to run GOTM-TOPAZ can be divided into the data needed to operate the GOTM and TOPAZ models  
142 individually. To run the GOTM, it is necessary to have the initial ocean data (temperature and salinity) and the salinity data  
143 for the duration of the model run time. The latter are needed to relax the GOTM. For TOPAZ, initial data are needed for the  
144 30 prognostic and 11 diagnostic tracers.

145

### 146 **4.2 Boundary Conditions**

147 Atmospheric forcing data must be prescribed in GOTM-TOPAZ because it is not coupled with an atmospheric model. The  
148 atmospheric forcing variables needed to run the model are: 10 m u-wind; v-wind [ $\text{m s}^{-1}$ ]; surface (2 m) air pressure [hPa];  
149 surface (2 m) air temperature [ $^{\circ}\text{C}$ ]; relative humidity [%], wet bulb temperature [ $^{\circ}\text{C}$ ], or dew point temperature [ $^{\circ}\text{C}$ ]; and  
150 cloud cover [1/10].

151 Values for surface or bottom fluxes for a few types of tracers must be provided to accurately simulate ocean  
152 biogeochemical variables. TOPAZ includes processes for variables including sediment calcite cycling and the external  
153 bottom fluxes of  $\text{O}_2$ ,  $\text{NH}_4$ ,  $\text{PO}_4$ , and alkalinity (Dunne et al., 2012b). However, it does not include a process for calculating

154 the atmosphere-ocean surface flux. Therefore, we added processes for calculating the surface fluxes of O<sub>2</sub>, NO<sub>3</sub>, NH<sub>4</sub>,  
 155 alkalinity, lithogenic aluminosilicate, dissolved iron, and dissolved inorganic carbon. Of the subroutines shown in Fig. 1., the  
 156 calculation of the surface fluxes is implemented using `generic_topaz_column_physics`. The surface flux of NO<sub>3</sub>, NH<sub>4</sub>,  
 157 lithogenic aluminosilicate, and dissolved iron is prescribed using monthly average climate values, while alkalinity is  
 158 calculated from prescribed NO<sub>3</sub> dry/wet deposition values. These surface flux data are provided by the Australian Research  
 159 Council's Centre of Excellence for Climate System Science (ARCCSS; <http://climate-cms.unsw.wikispaces.net/Data>). The  
 160 following equation was used to calculate the air-sea gas transfer for O<sub>2</sub> and CO<sub>2</sub> (dissolved inorganic carbon):

$$161$$

$$162 F = k_w \rho ([A] - [A]_{sat}) \quad (6)$$

$$163$$

164 Here,  $F$  is the upward flux of gas  $A$ , and  $k_w$  is its gas transfer velocity, which can be calculated as a function of the  
 165 Schmidt number and wind speed at 10 m (Wanninkhof, 1992).  $\rho$  is the density of surface seawater,  $[A]$  is the concentration  
 166 [ $\mu\text{mol kg}^{-1}$ ] of gas  $A$  at the surface of the ocean, and  $[A]_{sat}$  is the corresponding saturation concentration of gas  $A$  in  
 167 equilibrium with a water vapor-saturated atmosphere at total atmospheric pressure (Najjar and Orr, 1998).  $[A]$  is predicted by  
 168 the model. Please see Najjar and Orr (1998) for further detailed information related to Eq. (6).

169

### 170 4.3 Ocean Physics

171 The GOTM simulates the physics of oceanic environments based on Eqs. (1)–(4). In the coupled model, the GOTM relays  
 172 the following simulated one-dimensional ocean physical variables to the TOPAZ module at each time step: potential  
 173 temperature [ $^{\circ}\text{C}$ ]; salinity [psu]; thermal diffusion coefficient [ $\text{m}^2 \text{sec}^{-1}$ ]; density [ $\text{kg m}^{-3}$ ]; thickness [m]; mixed layer  
 174 thickness [m]; and radiation [ $\text{w m}^{-2}$ ].

175

### 176 4.4 Optical Feedback

177 As explained in Sect. 2, the photosynthesis of chlorophyll distributed throughout the upper ocean is known to have physical  
 178 effects. Manizza et al. (2005) used satellite observation data and OGCMs to conduct a study of changes in ocean irradiance  
 179 due to the absorption of visible light by chlorophyll. We used their methodology to apply the optical feedback from  
 180 chlorophyll on GOTM-TOPAZ in the following manner:

181

$$182 k_{\lambda} = k_{sw(\lambda)} + \chi_{(\lambda)} \cdot [chl]^{e_{(\lambda)}} \quad (7)$$

$$183 I_{IR} = I_0 \cdot 0.58 \quad (8)$$

$$184 I_{VIS} = I_0 \cdot 0.42 \quad (9)$$

$$185 \quad I_{RED} = I_{BLUE} = \frac{I_{VIS}}{2} \quad (10)$$

$$186 \quad I_{(z)} = I_{IR} \cdot e^{-k_{IRz}} + I_{RED(z-1)} \cdot e^{-k_{(r)}\Delta z} + I_{BLUE(z-1)} \cdot e^{-k_{(b)}\Delta z}. \quad (11)$$

187

188 In these equations, visible light was divided into red and blue/green bands in accordance with Manizza et al. (2005). In Eq.  
 189 (7),  $\lambda$  represents the wavelength of these bands and  $k_{sw(\lambda)}$  represents the light attenuation coefficient of optically pure  
 190 seawater, which has values of  $0.225 \text{ m}^{-1}$  and  $0.0232 \text{ m}^{-1}$ , respectively, in red and blue/green bands. In these bands, the  
 191 values of the pigment adsorption  $\chi_{(\lambda)}$  are  $0.037$  and  $0.074 \text{ m}^{-2} \text{ mg Chl m}^{-3}$ , respectively;  $e_{(\lambda)}$ , the power law for absorption,  
 192 has values of  $0.629$  and  $0.674$  [no units], respectively. Moreover, [chl] represents the concentration of chlorophyll in  
 193  $\text{mg Chl m}^{-3}$ .

194 Infrared light ( $I_{IR}$ ) and visible light ( $I_{VIS}$ ) that reach mean open ocean conditions are set in Eqs. (8) and (9), respectively,  
 195 by default. However, GOTM-TOPAZ can change the light extinction method by modifying the namelist in the GOTM (see  
 196 <http://www.gotm.net>) and this can also be used to change the coefficients of  $I_{IR}$  and  $I_{VIS}$ . The total irradiance of the red and  
 197 blue/green bands that reach the ocean surface is represented in Eq. (10). Ultimately, the irradiance of visible light transmitted  
 198 at each vertical level ( $z$ ) can be calculated in GOTM-TOPAZ using Eq. (11). Moreover, the sum of the second and third  
 199 terms on the right side of Eq. (11) represents photosynthetically active radiation (PAR) and is used in TOPAZ to calculate  
 200 the growth rate of phytoplankton groups.

201

## 202 4.5 w-advection

203 As mentioned at the beginning of Sect. 4, the upwelling phenomenon generated by coastal winds is known to affect  
 204 phytoplankton growth by supplying nutrient-rich intermediate water to the upper ocean. The GOTM is already designed to  
 205 allow users to prescribe w-advection to experiments. Therefore, we linked the subroutines of the GOTM that are related to  
 206 w-advection to TOPAZ, so GOTM-TOPAZ users can study the impact of upwelling on the biogeochemical environment of  
 207 the ocean. Users can prescribe vertical advection as a constant or input the velocities by time and depth in ASCII format to  
 208 reproduce the desired form of vertical motions. Please refer to the GOTM homepage (<http://www.gotm.net>) and Burchard et  
 209 al. (2006) for further technical details and numerical analysis of the w-advection in GOTM.

210

## 211 5 Experimental setup

212 The East/Japan Sea is unique, with its steep topography and three large, deep, and semi-enclosed basins. Moreover, it is  
 213 somewhat isolated from other major oceans, connects to the Pacific Ocean through a narrow strait, and is sometimes referred  
 214 to as a miniature ocean since it contains a double gyre and experiences various oceanic phenomena (Ichiye, 1984). The high-

215 temperature, high-salinity Tsushima Warm Current (TWC) introduced through the Korea Strait is divided into two main  
216 branches: the nearshore branch, which flows northeastward along the Japanese coast, and the East Korea Warm Current  
217 (EKWC), which flows northward along the Korean coast (Uda, 1934; Tanioka, 1968; Moriyasu, 1972) (Fig. 2). Apart from  
218 these two main branches, there is another that exists offshore of the first branch, but it is not present all year (Shimomura and  
219 Miyata, 1957; Kawabe, 1982). To the north, the North Korea Cold Current (NKCC) flows southward along the Korean coast.  
220 Furthermore, the 200–400 m East Sea Intermediate Water (ESIW) is known for its high concentration of dissolved oxygen  
221 and the appearance of a salinity-minimum layer (Kim and Chung, 1984; Kim and Kim, 1999). The East/Japan Sea is divided  
222 into warm and cold regions relative to the 40° N parallel, and, since the current pattern and characteristics of the East/Japan  
223 Sea vary spatially and seasonally, this region is very important to oceanographic studies. This region is also considered  
224 important for biogeochemical research (Joo et al., 2014; Kim et al., 2016; Shin et al., 2017) for the following reasons: the  
225 nutrient-rich seawater that flows along the southern coast of the Korean Peninsula due to inflow from the Nakdong River,  
226 which is located at its southeastern end; the influence of a strong southerly wind during the summer, which causes upwelling  
227 off the coast of the East/Japan Sea; and the transport of this nutrient- and chlorophyll-rich seawater near Ulleungdo Island by  
228 the EKWC. We selected three points that have features typical of the East/Japan Sea and for which observation data suitable  
229 to use for verification exist (Fig. 2): point 107, where the EKWC and NKCC meet (130.0° E, 38.0° N); point 104, which is  
230 an important location along the EKWC (131.3° E, 37.1° N); and point 102, which is in the middle of a warm eddy created as  
231 the EKWC moves north (130.6° E, 36.1° N). As noted previously, these points are in regions with strong advection and thus  
232 may not be suitable for testing GOTM-TOPAZ, which is an SCM. However, since the results obtained using GOTM-  
233 TOPAZ were significant when compared to the observations, we think that this shows that it is possible to perform  
234 sensitivity experiments using GOTM-TOPAZ at several kinds of locations.

235 The observed data, such as seawater temperature and salinity, were used to initialize and relax vertical structures in the  
236 GOTM throughout the simulation. These data were provided by the National Institute of Fisheries Science (NIFS;  
237 <http://www.nifs.go.kr/kodc>). The water temperature and salinity data from the NIFS were measured at 15-m intervals at  
238 depths of 0 m to 500 m. They were measured once in February, April, June, August, October, and December every year  
239 beginning in 1961. For the initial data on prognostic/diagnostic tracers in TOPAZ, we used the data provided by ARCCSS  
240 for use with MOM5 (<http://climate-cms.unsw.wikispaces.net/Data>). These initial tracer data were interpolated for each  
241 location, and a spin-up was applied over 14 years for use in the experiments. For atmospheric forcing data, we input 0.75°  
242 ERA-Interim reanalysis data provided by the European Centre for Medium Range Weather Forecasts (Dee et al., 2011). We  
243 applied global data to our model by interpolating the latitude and longitude values of the test points.

244 We used the monthly average of observed seawater temperature and salinity data from the analysis fields in the EN.4.2.1,  
245 provided by the Hadley Centre at the Met Office (Good et al., 2013), to verify the results from GOTM-TOPAZ following the  
246 adjusted method in Gouretski and Reseghetti (2010). With respect to chlorophyll, we compared the results simulated by the  
247 model using observational data with a resolution of 9 km gathered by the NASA Goddard Space Flight Center's Sea-  
248 Viewing Wide Field-of-View Sensor (SeaWiFS) from October 1997 to December 2007 (McClain et al., 1998). The results of



249 simulations of dissolved oxygen and nutrients such as nitrogen, phosphorus, and silicon were tested using observational data  
250 from the NIFS; these data were measured once every year, in February, April, June, August, October, and December, at  
251 depths of 0, 20, 50, and 100 m. Specific measurement dates and times were not fixed, so we viewed the measurement data as  
252 values that represented each month and used them to verify the model. Data from a model that operated MOM5, the Sea-Ice  
253 Simulator, and TOPAZ together (MOM) were used for comparative analysis. MOM was operated using CORE-II forcing  
254 data (Large and Yeager, 2009) from 1950 to 2008. We also used data from the Surface Ocean CO<sub>2</sub> Atlas (SOCAT) (Bakker  
255 et al., 2016) from the analysis period to verify the CO<sub>2</sub> air-sea gas flux in TOPAZ. The time periods for which SOCAT  
256 observational data exist for point 102 are April 2001, January 2005, November 2008, and December 2008. For points 104  
257 and 107, the time period is April 2001. Finally, we performed a spin-up for 14 years on the initial data at each point and  
258 analyzed the results of operating GOTM-TOPAZ from 1999 to 2008.

259

## 260 **6 Results**

261 Figure 3 shows the results of the GOTM-TOPAZ simulation and observational data (EN.4.2.1) as vertical distributions of the  
262 water column over time. The vertical distributions of salinity at all points are well simulated and are comparable to the  
263 observations, although this could also be because relaxation was applied. The water temperature at point 107, as simulated  
264 by GOTM-TOPAZ, showed a cold bias in the upper layer at a depth of around 120 m (Fig. 3a). This appears to be the effect  
265 of large-scale forcing (from the EKWC) that GOTM-TOPAZ could not resolve. **Similar differences in water temperature**  
266 **also appeared at points 104 and 102 (Fig. 3b and 3c).** Observational results showed that the water temperature was  
267 particularly affected by the ESIW, a finding that did not appear in the GOTM-TOPAZ results. **It was determined that since**  
268 **GOTM-TOPAZ could not reproduce advection from the ESIW, there were differences (warm bias) in the vertical water**  
269 **temperature distributions near depths of 200 m compared to the observational results at all points (Fig. 3).**

270 We used SeaWiFS data to measure chlorophyll concentrations using light reflected from the ocean surface and thus  
271 verified the results simulated by GOTM-TOPAZ. However, part of the reflected light reaches the satellite from the mixed  
272 layer below the ocean surface due to a backscattering effect (Jochum et al., 2009; Park et al., 2013). Therefore, we compared  
273 chlorophyll anomalies averaged up to 20 m in the data from each model and chlorophyll from SeaWiFS. **The mean**  
274 **chlorophyll concentration at depths of 0–20 m, as simulated by GOTM-TOPAZ and MOM, had similar seasonal variabilities**  
275 **at point 107; their correlation coefficients versus the observational data were 0.53 and 0.60, respectively, which is**  
276 **statistically significant ( $p < 0.001$ ) (Fig. 4a).** At points 104 and 102, these correlation coefficients of GOTM-TOPAZ versus  
277 the observational data were 0.25 ( $p < 0.01$ ) (Fig. 4c) and 0.32 ( $p < 0.001$ ) (Fig. 4e), respectively. In the case in which the  
278 maximum concentration of chlorophyll at all points occurred annually on the surface layer, GOTM-TOPAZ showed smaller  
279 errors against the observational results than did MOM (Fig. 4a, 4c, and 4e).

280 Phytoplankton in the East/Japan Sea are generally present in the highest concentrations at depths of around 10–60 m (Rho  
281 et al., 2012). Therefore, we averaged chlorophyll concentrations from 20–80 m to verify the model results (Fig. 4b, 4d and  
282 4f). However, since observational data for chlorophyll in the subsurface layer (~20–80 m) were unavailable, the MOM and  
283 GOTM-TOPAZ results were compared instead. There were slight differences in the scale of the minimum and maximum  
284 concentrations of chlorophyll in the subsurface layer at point 107, but the two models had a correlation coefficient of 0.59 ( $p$   
285  $< 0.01$ ) and a similar seasonal variability (Fig. 4b). At points 104 and 102, the GOTM-TOPAZ chlorophyll results had a  
286 slightly lower correlation coefficient against the observational data than MOM did, but its seasonal variability was similar to  
287 that of the observation data and the results from MOM (Fig. 4d and 4f). However, when compared to the results from MOM,  
288 the time series of the chlorophyll anomaly in the ocean surface and subsurface layers simulated by GOTM-TOPAZ appear to  
289 show a time shift (Fig. 4). In the TOPAZ module in MOM, the transport tendencies of each tracer were calculated in the  
290 ocean model; however, this process was not carried out in GOTM-TOPAZ. In addition, MOM and GOTM-TOPAZ are not  
291 only just different models of the marine physical environment; the atmospheric forcing data they each use are also different.  
292 Therefore, there are complex reasons for the differences in the results of the two models, and further detailed experiments  
293 and analysis are required.

294 We evaluated the performance of GOTM-TOPAZ in terms of simulations of dissolved oxygen, nitrogen, phosphorus, and  
295 silicon. The sea surface dissolved oxygen at point 107 simulated by GOTM-TOPAZ and MOM had correlation coefficients  
296 of 0.47 ( $p < 0.001$ ) and 0.50 ( $p < 0.001$ ), respectively, versus the observed data (Fig. 5a). The GOTM-TOPAZ correlation  
297 coefficient versus the observed data was 0.31 ( $p < 0.001$ ) for nitrogen, 0.16 ( $p < 0.10$ ) for phosphorus, and 0.19 ( $p < 0.05$ )  
298 for silicon; these were lower than the correlation coefficients between MOM and the observed data (0.36, 0.24, and 0.33,  
299 respectively;  $p < 0.001$ ). However, GOTM-TOPAZ seemed to depict the seasonal variability of nutrients at the sea surface  
300 well (Fig. 5b–d). At point 104, the GOTM-TOPAZ correlation coefficient was 0.37 ( $p < 0.001$ ) for dissolved oxygen, 0.54 ( $p$   
301  $< 0.001$ ) for nitrogen, 0.2 ( $p < 0.05$ ) for phosphorus, and 0.1 (statistically non-significant) for silicon (Fig. 6). For point 102,  
302 the GOTM-TOPAZ correlation coefficient was 0.59 ( $p < 0.001$ ) for dissolved oxygen, 0.24 ( $p < 0.01$ ) for nitrogen, 0.09  
303 (statistically non-significant) for phosphorus, and 0.2 ( $p < 0.01$ ) for silicon (Fig. 7). In these two points, GOTM-TOPAZ  
304 showed values for surface dissolved oxygen and nutrients with seasonal variabilities that were similar to those of the  
305 observed data and the data from MOM (Figs. 6–7).

306 Figures 8–10 show a comparison of the vertical profiles of dissolved oxygen, nitrogen, phosphorus, and silicon averaged  
307 for February, August, and the entire period from 1999 to 2008 at points 107, 104, and 102. Mixing in the upper ocean occurs  
308 actively during winter due to strong winds, and GOTM-TOPAZ simulated dissolved oxygen (surface to 250 m) and nitrogen  
309 (surface to 100 m) concentrations well during that season (Figs. 8–10a). However, for phosphorus and silicon at the same  
310 depths, there was a difference between the GOTM-TOPAZ results and the observational data. In the case of all points, the  
311 concentrations of nitrogen, phosphorus, and silicon simulated by GOTM-TOPAZ from the surface to 60 m decreased during  
312 August, and these concentrations were clearly distinguishable from each depth due to strong stratification in the summer  
313 (Figs. 8–10b). These stratifications appeared in the observational data. During this season, the oxygen concentration

314 simulated by GOTM-TOPAZ, increased sharply from depths of 20–60 m at points 107, 104, and 102 (Figs. 8–10b). This  
315 seems to have been caused by the creation of oxygen from photosynthesis by phytoplankton. However, a highly concentrated  
316 dissolved oxygen concentration is not apparent in the observational data, because the warm water, which is characterized by  
317 low dissolved oxygen, is transported by the EKWC during the summer season (Rho et al., 2012). The concentrations of  
318 dissolved oxygen from 80–250 m at point 107 were similar in both the results from GOTM-TOPAZ and in the 10-year  
319 observational data (Fig. 8c). However, the differences increased beyond depths of 250 m. Nonetheless, the results  
320 demonstrated that dissolved oxygen at 80–250 m, nitrogen, and phosphorus (but not silicon) are well simulated over 10 years  
321 using GOTM-TOPAZ (Fig. 8c). The vertical distributions of dissolved oxygen and nutrients at points 104 and 102 as  
322 simulated by GOTM-TOPAZ over the same time period also showed similar patterns as those at point 107 (Figs. 9–10).

323 In addition, the magnitudes of the source and sink terms of GOTM-TOPAZ were analyzed. When TOPAZ was  
324 implemented three-dimensionally by being coupled with MOM, the concentration of tracers was calculated through  
325 advection-diffusion processes as well as source/sink processes. On the other hand, in the case of GOTM-TOPAZ, which is  
326 an SCM, it determined the tendency of state variables through vertical diffusion and source and sink terms without  
327 considering advection and horizontal diffusion. At every point, the bias of dissolved oxygen seemed to be larger in summer  
328 than in winter, where the vertical diffusion is stronger. Since there was a bias also in the deep sea (< 250 m), we focused on  
329 source and sink terms rather than on vertical diffusion. Figures 11–13 show 10-year average source and sink terms (1999–  
330 2008) of nutrients (nitrate, phosphate, silicate) and dissolved oxygen. The production of dissolved oxygen is attributable to  
331 nitrate, ammonia, and nitrogen fixation, while its loss occurs in the production of  $\text{NH}_4$  from non-sinking particles, sinking  
332 particles, and dissolved organic matter and nitrification. The production of nitrate is caused by nitrification, and its loss is  
333 determined by denitrification and uptake by phytoplankton. In the phosphate and silicate, the production is attributable to  
334 dissolved organic matter and particles, and the loss is determined by uptake due to phytoplankton (Dunne et al., 2012b).

335 As shown in Figures 11–13, the source and sink of dissolved oxygen and nutrients occurred mainly in the surface layer (<  
336 60 m), and their influence seemed to be negligible at deeper depths. The source of dissolved oxygen was remarkable in the  
337 surface layer during summer, because phytoplankton flourishes in summer. This pattern was commonly observed at all three  
338 points. The surface layer of point 102, which is the southernmost point, showed more production (consumption) of dissolved  
339 oxygen (nutrients) than did the other points in winter. Being located at the southernmost location, point 102 was greatly  
340 affected by the warm current (EKWC), which resulted in flourishing phytoplankton. However, even at this point, the source  
341 and sink of both the dissolved oxygen and nutrients made few contributions at 250 m or deeper.

342 Accordingly, it could be inferred that the simulation of biogeochemical variables in the deep sea (< 250 m) would be more  
343 affected by initial values than by source/sink. In order to verify this assumption, the model was simulated by setting the  
344 initial data as the observations. The results indicated that the bias of dissolved oxygen was significantly reduced in the deep  
345 sea (Fig. 14). This result indicates that tracers simulated by GOTM-TOPAZ greatly depend on source/sink processes in the  
346 surface layer (< 60 m) and are sensitive to initial values in the deep sea.

347 Finally, to verify the air-sea gas exchange simulated by GOTM-TOPAZ, we compared the monthly average sea surface  
348 CO<sub>2</sub> concentrations in the model and in SOCAT. The correlation coefficient between the sea surface CO<sub>2</sub> concentration  
349 simulated by GOTM-TOPAZ and the observational data was 0.94 (Fig. 15). However, there were no more than six months  
350 for which the observational values existed at all points; therefore, this is a statistically insignificant value.  
351

## 352 **7 Discussion**

353 In this paper, we explain the major models that comprise GOTM-TOPAZ and the biological-physical feedback loop that they  
354 reproduce. In addition, we compiled data from three points of scientific importance in the East/Japan Sea, near the Korean  
355 Peninsula and analyzed the results of operating GOTM-TOPAZ for a decade (~1999–2008). We compared ocean water  
356 temperatures, salinity, and biogeochemical variables such as chlorophyll, dissolved oxygen, nitrogen, phosphorus, and  
357 silicon concentrations against the observational data and output from the OGCM to evaluate the performance of GOTM-  
358 TOPAZ. The results showed that GOTM-TOPAZ had lower correlation coefficients than did OGCM but that it simulated  
359 seasonal variability in a similar manner overall. **In addition, we analyzed the magnitudes of the source/sink terms for  
360 dissolved oxygen and nutrients, which were simulated by GOTM-TOPAZ. This analysis revealed the characteristics of the  
361 model and the cause of the bias, which was shown in the vertical profile of dissolved oxygen. Consequently, GOTM-TOPAZ  
362 is mainly affected by source/sink terms in the surface layer (< 60 m) and is sensitive to initial values in the deep sea (> 250  
363 m). Future users of GOTM-TOPAZ need to consider such characteristics when designing an experiment.**

364 The SCM (1D model) includes important physical processes and has a much lower computation cost than do the 3D  
365 models; this means that a variety of experiments can be performed repeatedly. With this advantage, 1D models can be useful  
366 to track mechanisms that are difficult to understand using 3D models. We believe that TOPAZ, in particular, can be used to  
367 obtain insights on the interactions between the chemical makeup and organisms in the ocean because it accounts for complex  
368 biogeochemical mechanisms. In addition, the key processes which are studied via TOPAZ can later be implemented into 3D  
369 models.

370 A variety of single-column ocean biogeochemical models have already been developed. However, GOTM-TOPAZ  
371 includes complex biogeochemical processes and models over 30 kinds of tracers; the other models, which have only simple  
372 structures, do not (Dunne et al., 2012b). Furthermore, GOTM-TOPAZ considers the gas transfer caused by changes in the  
373 atmosphere and the physical environment of the ocean, depicting the deposition of dissolved iron, lithogenic aluminosilicate,  
374 NH<sub>4</sub>, and NO<sub>3</sub> due to aerosols. We believe that the sophistication of TOPAZ provides researchers with the opportunity to  
375 perform a variety of experiments.

376 For example, aerosol concentrations are continuously increasing over the East Asia region and are known to affect  
377 precipitation and atmospheric circulation. Thus, there is a possibility that aerosols affect oceanic biogeochemical processes  
378 as deposition occurs into the ocean, and this cannot be ignored. A variety of numerical experiments are necessary to

379 understand this process, but they are difficult to perform using 3D models due to limitations in computing resources.  
380 However, as previously noted, GOTM-TOPAZ is fast; as such, it is useful for understanding the biogeochemical changes  
381 that occur in the ocean when the concentration of aerosols or CO<sub>2</sub> in the atmosphere changes. In addition, recent studies have  
382 reported that the distribution of fisheries is changing due to changes in phytoplankton size structure caused by the upwelling  
383 intensity on the coast of the East/Japan Sea (Shin et al., 2017). The TOPAZ phytoplankton are divided into two types  
384 depending on their size, which should prove to be useful in this type of future research.

385 In addition, GOTM-TOPAZ can be used in studies on feedback mechanisms in the biogeochemical and physical  
386 environment of the ocean. Sonntag and Hense (2011) used a simple biogeochemistry model linked to GOTM (GOTM-BIO)  
387 to analyze the effects of phytoplankton on the physical environment of the upper ocean. The feedback from cyanobacteria,  
388 particularly during surface blooms that cause changes in ocean surface albedo, the solar light absorption rate, and the  
389 momentum relayed to the ocean by wind were applied to the model during the experiment. Sonntag and Hense (2011)  
390 provided us a better understanding of the needs and direction to focus on with GOTM-TOPAZ, and we plan to apply various  
391 climate-ocean biogeochemistry feedback mechanisms to it in future research. We also plan to evolve GOTM-TOPAZ into a  
392 single ESM by coupling an atmospheric SCM and a model that reproduces atmospheric chemical mechanisms with GOTM-  
393 TOPAZ.

394 We separated TOPAZ from MOM and constructed a model with separate initiation and column physics modules, thus  
395 introducing the possibility of more easily coupling it with various other ocean models in the future. We are currently  
396 conducting a study on coupling TOPAZ with the Nucleus for European Modelling of the Ocean (NEMO), another OGCM  
397 that is already coupled with other biogeochemistry models, such as the MEDUSA (Yool et al., 2013) and the PISCES  
398 (Aumont et al., 2015). If NEMO and TOPAZ can be coupled successfully, a comparative analysis of the simulation results  
399 from the each biogeochemistry model might provide the driving force for improving the modelling of physical processes  
400 associated with ocean-biogeochemistry.

401

#### 402 **Code and data availability:**

403 The GOTM-TOPAZ software is based on GOTM version 4 and MOM version 5, both available for download from their  
404 respective distribution sites (<https://gotm.net>, <https://www.gfdl.noaa.gov/>). GOTM-TOPAZ is freely available at  
405 <https://doi.org/10.5281/zenodo.1405270>.

406

407 **Author contribution:**

408 H.C.J. and B.K.M. drafted the paper, performed the experiments, and were primarily responsible for developing GOTM-  
409 TOPAZ. J.W., H.S.P., J.L., and Y.H.B. contributed to code debugging and writing the paper.

410

411 **Competing interests:**

412 The authors declare that they have no conflicts of interest.

413

414 **Acknowledgements:**

415 We would like to thank the GOTM and MOM communities for their support. In addition, we would like to thank the  
416 European Centre for Medium Range Weather Forecasts for providing ERA-Interim data and the Hadley Centre at the Met  
417 Office for providing the EN4 datasets. In addition, we would like to thank the National Institute of Fisheries Science for  
418 providing ocean observation data and the NASA Goddard Space Flight Center for providing SeaWiFS datasets. We also  
419 thank D.H. Kim at Kongju National University of Korea for providing some advice during this research. We appreciate J.H.  
420 Choi and H.K. Kim at Chonbuk National University of Korea for their helpful discussion and comments. This work was  
421 funded by the Korea Meteorological Administration Research and Development Program under Grant KMI (KMI2018-  
422 03513).

423

424 **References**

- 425 Aumont, O., Ethe, C., Tagliabue, A., Bopp, L., and Gehlen, M.: PISCES-v2: an ocean biogeochemical model for carbon and  
426 ecosystem studies, *Geosci. Model Dev.*, 8, 2465–2513, doi:10.5194/gmd-8-2465-2015, 2015.
- 427 Azhar, M. A., Canfield, D. E., Fennel, K., Thamdrup, B., and Bjerrum, C. J.: A model-based insight into the coupling of  
428 nitrogen and sulphur cycles in a coastal upwelling system, *J. Geophys. Res. Biogeosci.*, 119, 264–285,  
429 doi:10.1002/2012JG002271, 2014.
- 430 Bakker, D. C. E., Pfeil, B., Landa, C. S., Metzl, N., O'Brien, K. M., Olsen, A., Smith, K., Cosca, C., Harasawa, S., Jones, S.  
431 D., Nakaoka, S.-I., Nojiri, Y., Schuster, U., Steinhoff, T., Sweeney, C., Takahashi, T., Tilbrook, B., Wada, C.,  
432 Wanninkhof, R., Alin, S. R., Balestrini, C. F., Barbero, L., Bates, N. R., Bianchi, A. A., Bonou, F., Boutin, J., Bozec, Y.,  
433 Burger, E. F., Cai, W.-J., Castle, R. D., Chen, L., Chierici, M., Currie, K., Evans, W., Featherstone, C., Feely, R. A.,  
434 Fransson, A., Goyet, C., Greenwood, N., Gregor, L., Hankin, S., Hardman-Mountford, N. J., Harlay, J., Hauck, J.,  
435 Hoppema, M., Humphreys, M. P., Hunt, C. W., Huss, B., Ibáñez, J. S. P., Johannessen, T., Keeling, R., Kitidis, V.,  
436 Körtzinger, A., Kozyr, A., Krasakopoulou, E., Kuwata, A., Landschützer, P., Lauvset, S. K., Lefèvre, N., Lo Monaco, C.,  
437 Manke, A., Mathis, J. T., Merlivat, L., Millero, F. J., Monteiro, P. M. S., Munro, D. R., Murata, A., Newberger, T., Omar,  
438 A. M., Ono, T., Paterson, K., Pearce, D., Pierrot, D., Robbins, L. L., Saito, S., Salisbury, J., Schlitzer, R., Schneider, B.,  
439 Schweitzer, R., Sieger, R., Skjelvan, I., Sullivan, K. F., Sutherland, S. C., Sutton, A. J., Tadokoro, K., Telszewski, M.,  
440 Tuma, M., van Heuven, S. M. A. C., Vandemark, D., Ward, B., Watson, A. J., and Xu, S.: A multi-decade record of high-  
441 quality fCO<sub>2</sub> data in version 3 of the Surface Ocean CO<sub>2</sub> Atlas (SOCAT), *Earth Syst. Sci. Data*, 8, 383–413,  
442 <https://doi.org/10.5194/essd-8-383-2016>, 2016.
- 443 Betts, A. K., and Miller, M. J.: A new convective adjustment scheme. Part II: Single column tests using GATE wave,  
444 BOMEX, ATEX and arctic air-mass data sets, *Q. J. Roy. Meteor. Soc.*, 112, 693–709, doi:10.1002/qj.49711247308,  
445 1986.
- 446 Bruggenman, J., and Bolding, K.: A general framework for aquatic biogeochemical models, *Environ. Modell. Softw.*, 61,  
447 249–265, doi:10.1016/j.envsoft.2014.04.002, 2014.
- 448 Burchard, H., Bolding, K., Kuhn, W., Meister, A., Neumann, T., and Umlauf, L.: Description of a flexible and extendable  
449 physical-biogeochemical model system for the water column, *J. Marine Syst.*, 61, 180–211,  
450 doi:10.1016/j.jmarsys.2005.04.011, 2006.
- 451 Cloern, J. E., Grenz, C., and Videgar-Lucas, L.: An empirical model of the phytoplankton chlorophyll: carbon ratio-the  
452 conversion factor between productivity and growth rate, *Limnol. Oceanogr.*, 40(7), 1313–1321,  
453 doi:10.4319/lo.1995.40.7.1313, 1995.
- 454 De Baar, H. J. W.: von Liebig's law of the minimum and plankton ecology (1899-1991), *Progress. Oceanogr.*, 33, 347–386,  
455 1994.

456 Dee, D. P., Uppala, S. M., Simmons, A. J., Berrisford, P., Poli, P., Kobayashi, S., Andrae, U., Balmaseda, M. A., Balsamo,  
457 G., Bauer, P., Bechtold, P., Beljaars, A. C. M., van de Berg, L., Bidlot, J., Bormann, N., Delsol, C., Dragani, R., Fuentes,  
458 M., Geer, A. J., Haimberger, L., Healy, S. B., Hersbach, H., Hólm, E. V., Isaksen, I., Kållberg, P., Köhler, M.,  
459 Matricardi, M., McNally, A. P., Monge-Sanz, B. M., Morcrette, J.-J., Park, B.-K., Peubey, C., de Rosnay, P., Tavolato,  
460 C., Thépaut, J.-N., and Vitart, F.: The ERA-Interim reanalysis: configuration and performance of the data assimilation  
461 system, *Q. J. Royal Meteorol. Soc.*, 137, 553–597, doi:10.1002/qj.828, 2011.

462 Dirmeyer, P. A., Cash, B. A., Kinter III, J. L., Stan, C., Jung, T., Marx, L., Towers, P., Wedi, N., Adams, J. M., Altshuler, E.  
463 L., Huang, B., Jin, E. K., and Manganello, J.: Evidence for enhanced land-atmosphere feedback in a warming climate, *J.*  
464 *Hydrometeorol.*, 13, 981–995, doi:10.1175/JHM-D-11-0104.1, 2012.

465 Dunne, J. P., John, J. G., Adcroft, A. J., Griffies, S. M., Hallberg, R. W., Shevliakova, E. N., Stouffer, R. J., Cooke, W.,  
466 Dunne, K. A., Harrison, M. J., Krasting, J. P., Malyshev, S. L., Milly, P. C. D., Phillipps, P. J., Sentman, L. A., Samuels,  
467 B. L., Spelman, M. J., Winton, M., Wittenberg, A. T., and Zadeh, N.: GFDL’s ESM2 global coupled climate-carbon  
468 Earth System Models Part I: Physical formulation and baseline simulation characteristics, *J. Clim.*, doi:10.1175/JCLI-D-  
469 11-00560.1, 2012a.

470 Dunne, J. P., John, J. G., Shevliakova, E., Stouffer, R. J., Krasting, J. P., Malyshev, S. L., Milly, P. C. D., Sentman, L. T.,  
471 Adcroft, A. J., Cooke, W., Dunne, K. A., Griffies, S. M., Hallberg, R. W., Harrison, M. J., Levy, H., Wittenberg, A. T.,  
472 Phillips, P. J., and Zadeh, N.: GFDL’s ESM2 global coupled climate–carbon earth system models. Part II: carbon system  
473 formulation and baseline simulation characteristics, *J. Clim.*, 26, 2247–2267, doi:10.1175/jcli-d-12-00150.1, 2012b.

474 Evans, T., and Garçon, V.: One-Dimensional Models of Water Column Biogeochemistry; Report of a Workshop held in  
475 Toulouse, France; November-December 1995, 1997.

476 Friedlingstein, P., Cox, P., Betts, R., Bopp, L., von Bloh, W., Brovkin, V., Cadule, P., Doney, S., Eby, M., Fung, I., Bala, G.,  
477 John, J., Jones, C., Joos, F., Kato, T., Kawamiya, M., Knorr, W., Lindsay, K., Matthews, H. D., Raddatz, T., Rayner, P.,  
478 Reick, C., Roeckner, E., Schnitzler, K. G., Schnur, R., Strassmann, K., Weaver, A. J., Yoshikawa, C., and Zeng, N.:  
479 Climate-Carbon Cycle Feedback Analysis: Results from the C4MIP Model Intercomparison, *J. Clim.*, 19(14), 3337–3353,  
480 doi:10.1175/JCLI3800.1, 2006.

481 Good, S. A., Martin, M. J., and Rayner, N. A.: EN4: Quality controlled ocean temperature and salinity profiles and monthly  
482 objective analyses with uncertainty estimates, *J. Geophys. Res. Oceans*, 118, 6704–6716, doi:10.1002/2013JC009067,  
483 2013.

484 Gouretski, V., and Reseghetti, F.: On depth and temperature biases in bathythermograph data: development of a new  
485 correction scheme based on analysis of a global ocean database, *Deep-Sea Res. Pt. I*, 57, 6, doi:10.1016/j.dsr.2010.03.011,  
486 2010.

487 Hartung, K., Svensson, G., Struthers, H., Deppenmeier, A., and Hazeleger, W.: An EC-Earth coupled atmosphere-ocean  
488 single-column model (AOSCM) for studying coupled marine and polar process, *Geosci. Model Dev. Discuss.*,  
489 doi:10.5194/gmd-2018–66, 2018.



490 Hense, I., Stemmler, I., and Sonntag, S.: Ideas and perspectives: climate-relevant marine biologically driven mechanisms in  
491 Earth system models, *Biogeosciences*, 14, 403–413, doi:10.5194/bg-14-403-2017, 2017.

492 Ichiye, T.: Some problem of circulation and hydrography of the Japan Sea and Tsushima Current. In: *Ocean Hydrography of*  
493 *the Japan Sea and China Seas*, edited by: Ichiye, T., Elsevier Science Publishers, Amsterdam, 15–54, 1984.

494 Jochum, M., Yeager, S., Lindsay, K., Moore K., and Murtugudde, R.: Quantification of the Feedback between  
495 Phytoplankton and ENSO in the Community Climate System Model, *J. Clim.*, 23, 2916–2925,  
496 doi:10.1175/2010JCLI3254.1, 2009.

497 Jones, C., and Sellar, A.: Development of the 1st version of the UK Earth system model, UKESM newsletter no. 1 – August  
498 2015, available at: <https://ukesm.ac.uk/ukesm-newsletter-no-1-august-2015/> (last accessed: 4 November 2018), 2015.

499 Joo, H. T., Park, J. W., Son, S. H., Noh, J.-H., Jeong, J.-Y., Kwak, J. H., Saux-Picart, S., Choi, J. H., Kang, C.-K., and Lee,  
500 S. H.: Long-term annual primary production in the Ulleung Basin as a biological hot spot in the East/Japan Sea, *J.*  
501 *Geophys. Res. Oceans*, 119, 3002–3011, doi:10.1002/2014JC009862, 2014.

502 Kawabe, M. Branching of the Tsushima Current in the Japan Sea. Part II: Numerical experiment, *J. Oceanogr. Soc. Japan*, 38,  
503 183–192, doi:10.1007/BF02111101, 1982.

504 Kim, D.-W., Jo, Y.-H., Choi, J.-K., Choi, J.-G., and Bi, H.: Physical processes leading to the development of an anomalously  
505 large *Cochlodinium polykrikoides* bloom in the East sea/Japan sea, *Harmful Algae*, 55, 250–258,  
506 doi:10.1016/j.hal.2016.03.019, 2016.

507 Kim, K., and Chung, J. Y.: On the Salinity-Minimum and Dissolved Oxygen-Maximum Layer in the East Sea (Sea Of  
508 Japan), *Elsevier Oceanogr. Ser.*, 39, 55–65, doi:10.1016/S0422-9894(08)70290-3, 1984.

509 Kim, Y.-G., and Kim, K.: Intermediate Waters in the East/Japan Sea, *J. Oceanogr.*, 55, 123–132,  
510 doi:10.1023/A:1007877610531, 1999.

511 Krezel, A., Szymanek, L., Kozłowski, L., and Szymelfenig, M.: Influence of coastal upwelling on chlorophyll a  
512 concentration in the surface water along the Polish coast of the Baltic Sea, *Oceanologia*, 47(4), 433–452, 2005.

513 Large, W. G. and Yeager, S. G.: The global climatology of an interannually varying air-sea flux data set, *Clim. Dyn.*, 33,  
514 341–364, doi:10.1007/s00382-008-0441-3, 2009.

515 Lebassi-Habtezion, B., and Caldwell, P. M.: Aerosol specification in single-column Community Atmosphere Model version  
516 5, *Geosci. Model Dev.*, 8, 817–828, doi:10.5194/gmd-8-817-2015, 2015.

517 Lim, H.-G., Park, J.-Y., and Kug, J.-S.: Impact of chlorophyll bias on the tropical Pacific mean climate in an earth system  
518 model, *Clim. Dyn.*, doi:10.1007/s00382-017-4036-8, 2017.

519 Lips, I., and Lips, U.: Phytoplankton dynamics effected by the coastal upwelling events in the Gulf of Finland in July-August  
520 2006, *J. Plankton Res.*, 32(9), 1269–1282, doi:10.1093/plankt/fbq049, 2010.

521 Litchman, E., Pinto, P. T., Edwards, K. F., Klausmeier, C. A., Kremer, C. T., and Thomas M. K.: Global biogeochemical  
522 impacts of phytoplankton: a trait-based perspective, *J. Ecol.*, 103, 1384–1396, doi:10.1111/1365-2745.12438, 2015.

523 Manizza, M., Le Quéré, C., Watson, A. J., and Buitenhuis, E. T.: Bio-optical feedbacks among phytoplankton, upper ocean  
524 physics and sea-ice in a global model, *Geophys. Res. Lett.*, 32, L05603, doi:10.1029/2004GL020778, 2005.

525 McClain, C. R., Cleave, M. L., Feldman, G. C., Gregg, W. W., Hooker, S. B., and Kuring, N.: Science quality seawifs data  
526 for global biosphere research, *Sea Technol.*, 39, 10–16, 1998.

527 Morel, A., and Antoine, D.: Heating rate within the upper ocean in relation to its Bio-Optical state, *J. Phys. Oceanogr.*, 24,  
528 1652–1665, doi:10.1175/1520-0485(1994)024<1652:HRWTUO>2.0.CO;2, 1994.

529 Moriyasu, S.: The Tsushima Current. Kuroshio, Its Physical Aspects, 353–369 pp., 1972.

530 Najjar, R., and Orr, J. C.: Design of OCMIP-2 simulations of chlorofluorocarbons, the solubility pump and common  
531 biogeochemistry, Internal report of the Ocean Carbon-Cycle Model Intercomparison Project (OCMIP), 25 pp.,  
532 LSCE/CEA Saclay, Gif-sur-Yvette, France, 1998.

533 National Institute of Fisheries Science (NIFS), Korea Oceanographic Data Center, <http://www.nifs.go.kr/kodc>. (accessed  
534 May 20, 2018)

535 Park, J.-Y., Dunne, J. P., and Stock, C. A.: Ocean chlorophyll as a precursor of ENSO: An Earth system modeling study,  
536 *Geophys. Res. Lett.*, 45, 1939–1947, doi:10.1002/2017GL076077, 2018.

537 Park, J.-Y., Kug, J.-S., Seo, H., and Bader, J.: Impact of bio-physical feedbacks on the tropical climate in coupled and  
538 uncoupled GCMs, *Clim. Dyn.*, 43, 1811–1827, doi:10.1007/s00382-013-2009-0, 2013.

539 Price, J. F., Weller, R. A., and Pinkel, R.: Diurnal cycling: Observations and models of the upper ocean response to diurnal  
540 heating, cooling, and wind mixing, *J. Geophys. Res. Oceans*, 91, 8411–8427, doi:10.1029/JC091iC07p08411, 1986.

541 Randerson, J. T., Lindsay, K., Munoz, E., Fu, W., Moore, J. K., Hoffman, F. M., Mahowald, N. M., and Doney, S. C.:  
542 Multicentury changes in ocean and land contributions to the climate-carbon feedback, *Global Biogeochem. Cycles*, 29,  
543 744–759, doi:10.1002/2014GB005079, 2015.

544 Redfield, A. C., Ketchum, B. H., and Richards, F.: The influence of organisms on the composition of sea water, in: *The Sea*,  
545 edited by: Hill, M. N., Wiley-Interscience, New York, 2, 26–77, 1963.

546 Rho, T., Lee, T., Kim, G., Chang, K.-I., Na, T., and Kim, K.-R.: Prevailing Subsurface Chlorophyll Maximum (SCM) Layer  
547 in the East Sea and Its Relation to the Physico-Chemical Properties of Water Masses, *Ocean and Polar Res.*, 34(4), 413–  
548 430, doi:10.4217/OPR.2012.34.4.413, 2012. (in Korean)

549 Sauerland, V., Löptien, U., Leonhard, C., Oschlies, A., and Srivastav, A.: Error assessment of biogeochemical models by  
550 lower bound methods (NOMMA-1.0), *Geosci. Model Dev.*, 11, 1181–1198, doi:10.5194/gmd-11-1181-2018, 2018.

551 Shimomura, T. and Miyata K. The oceanographical conditions of the Japan sea and its water systems, laying stress on the  
552 summer of 1955, *Bull. Japan Sea Reg. Fish. Res. Lab.*, 6, 23–97, 1957. (in Japanese)

553 Shin, J.-W., Park, J., Choi, J.-G., Jo, Y.-H., Kang, J. J., Joo, H. T., and Lee, S. H.: Variability of phytoplankton size structure  
554 in response to changes in coastal upwelling intensity in the southwestern East Sea, *J. Geophys. Res. Oceans*, 122, 10,  
555 262–10, 274, doi:10.1002/2017JC013467, 2017.

556 Soden, B. J., and Held, I. M.: An assessment of Climate Feedbacks in Coupled Ocean-Atmosphere Models, *J. Clim.*, 19(14),  
557 3354, doi:10.1175/JCLI3799.1, 2006.

558 Sokolov, A., Kicklighter, D., Schlosser, C. A., Wang, C., Monier, E., Brown-Steiner, B., Prinn, R., Forest, C., Gao, X.,  
559 Libardoni, A., and Eastham, S.: Description and Evaluation of the MIT Earth System Model (MESH), *J. Adv. Model.*  
560 *Earth. Sy.*, 10(8), 1759–1789, doi:10.1029/2018MS001277, 2018.

561 Sonntag, S., and Hense, I.: Phytoplankton behavior affects ocean mixed layer dynamics through biological-physical  
562 feedback mechanisms, *Geophys. Res. Lett.*, 38, L15610, doi:10.1029/2011GL048205, 2011.

563 Stock C. A., Dunne, J. P., and John, J. G.: Global-scale carbon and energy flows through the marine planktonic food web: an  
564 analysis with a coupled physical–biological model, *Progr. Oceanogr.*, 120, 1–28, doi:10.1016/j.pocean.2013.07.001, 2014.

565 Tanioka, K.: On the Eastern Korea Warm Current (Tosen Warm Current), *Oceanogr. Mag.*, 20, 31–38, 1968.

566 Uda, M.: The results of simultaneous oceanographical investigations in the Japan Sea and its adjacent waters in May and  
567 June 1932, *J. Imp. Fisher. Exp. St.*, 5, 57–190, 1934. (in Japanese)

568 Umlauf, L., and Burchard, H.: A generic length-scale equation for geophysical turbulence models, *J. Mar. Res.* 61, 235–265,  
569 doi:10.1357/002224003322005087, 2003.

570 Umlauf, L., and Burchard, H.: Second-order turbulence closure models for geophysical boundary layers. A review of recent  
571 work, *Cont. Shelf Res.*, 25, 795–827, doi:10.1016/j.csr.2004.08.004, 2005.

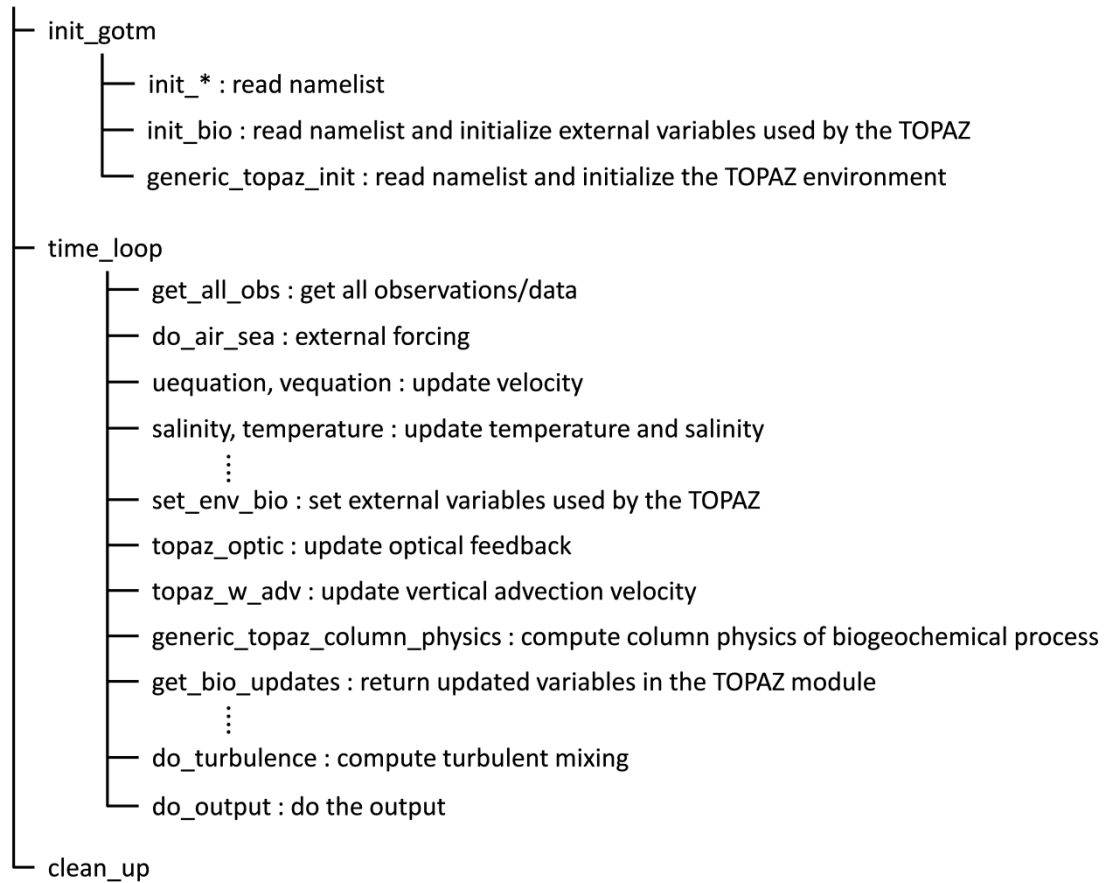
572 Umlauf, L., Burchard, H., and Bolding, K.: General Ocean Turbulence Model. Scientific documentation. v3.2. Marine  
573 Science Reports no. 63, Baltic Sea Research Institute Warnemünde, 274 pp., Warnemünde, Germany, 2005.

574 Wanninkhof, R.: Relationship between wind speed and gas exchange over the ocean, *J. Geophys. Res.*, 97, 7373–7382,  
575 doi:10.1029/92JC00188, 1992.

576 Yool, A., Popova, E. E., and Anderson, T. R.: MEDUSA-2.0: an intermediate complexity biogeochemical model of the  
577 marine carbon cycle for climate change and ocean acidification studies, *Geosci. Model Dev.*, 6, 1767–1811,  
578 doi:10.5194/gmd-6-1767-2013, 2013.

579  
580  
581

## GOTM-TOPAZ



583

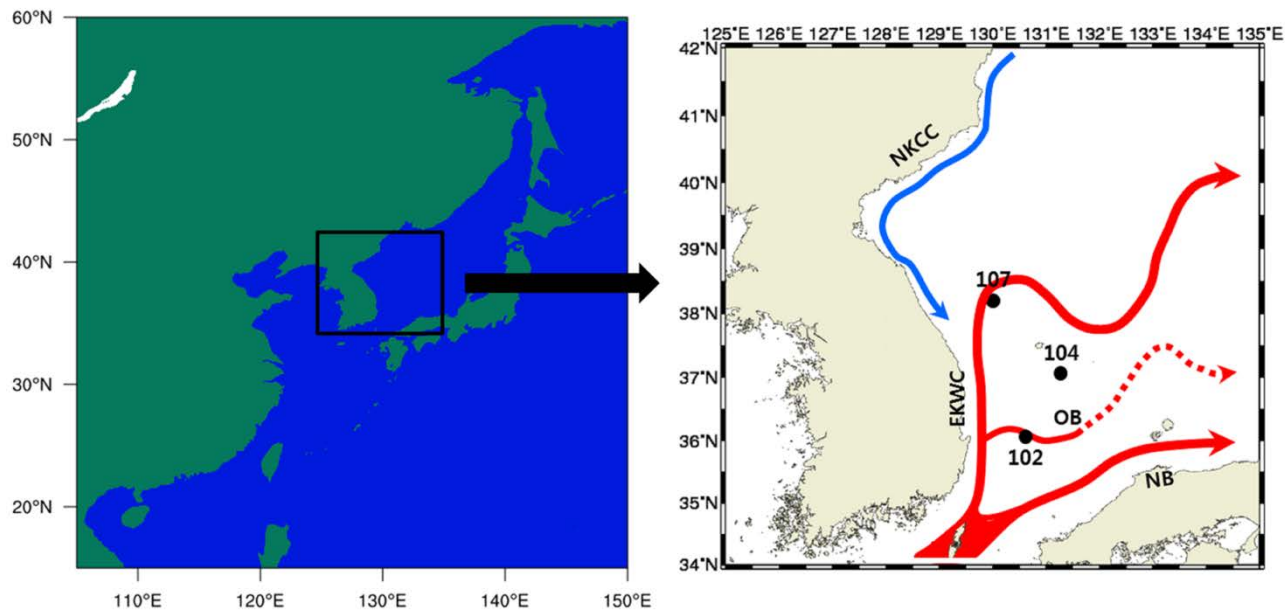
584 **Figure 1: Flow diagram of the Fortran subroutines comprising the Generic Ocean Turbulence Model-Tracers of Phytoplankton**  
 585 **with Allometric Zooplankton**

586

587

588

589

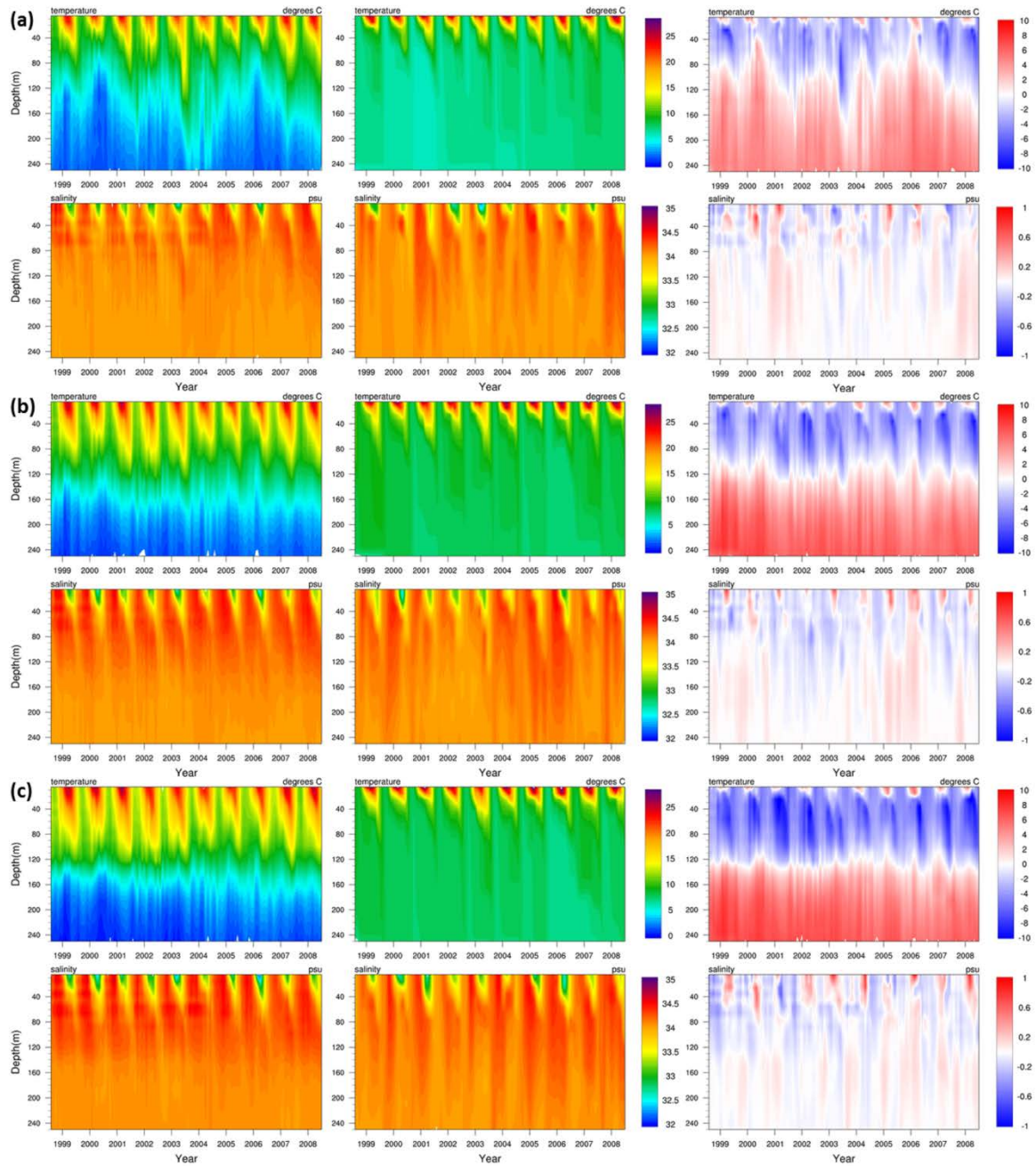


590

591 **Figure 2: Location of points (107, 104, 102) in the East/Japan Sea and flow of the nearby North Korea Cold Current (NKCC), East**  
592 **Korea Warm Current (EKWC), Offshore Branch (OB) of the Tsushima Warm Current, and the Nearshore Branch (NB) of the**  
593 **Tsushima Warm Current.**

594

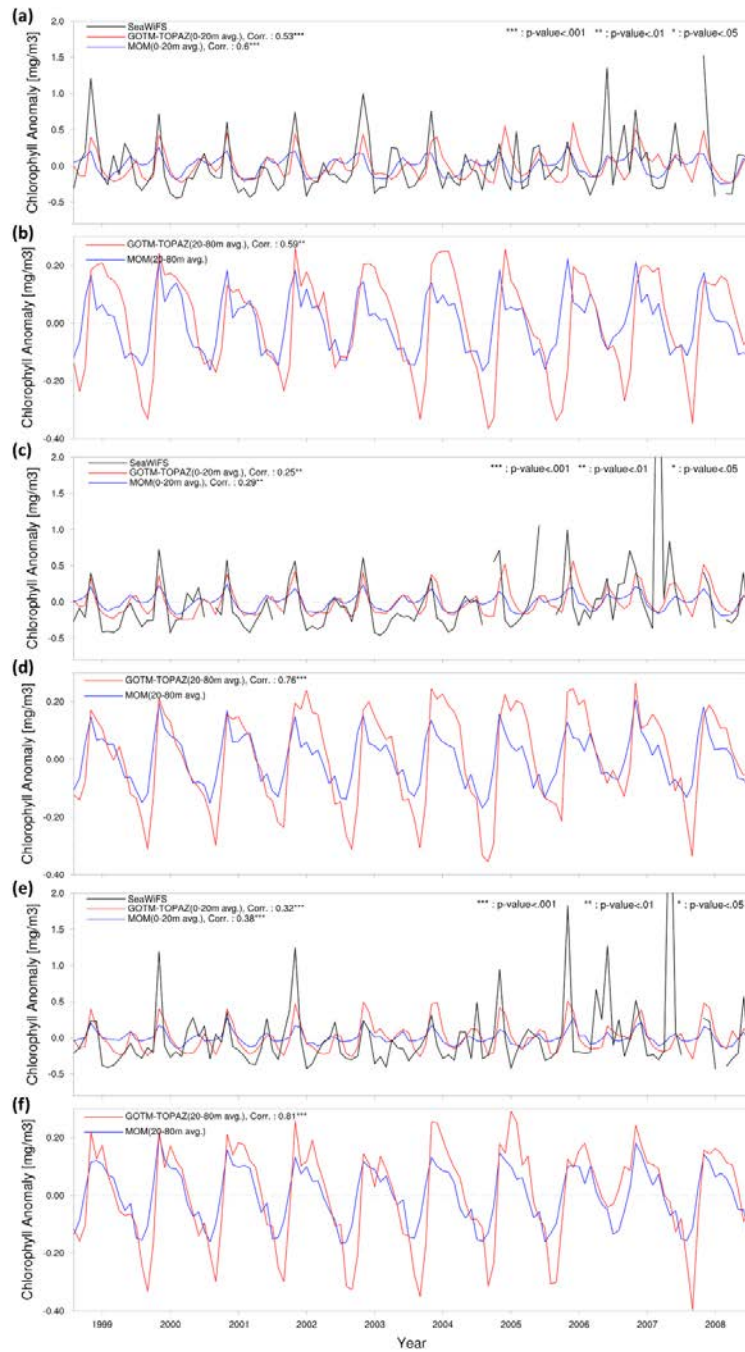
595

597  
598  
599

**Figure 3: Comparison of the vertical distribution for water temperature [°C], salinity [psu], and the difference (GOTM-TOPAZ minus the observations) at points (a) 107, (b) 104, and (c) 102 for the 10-year period (1999–2008).**

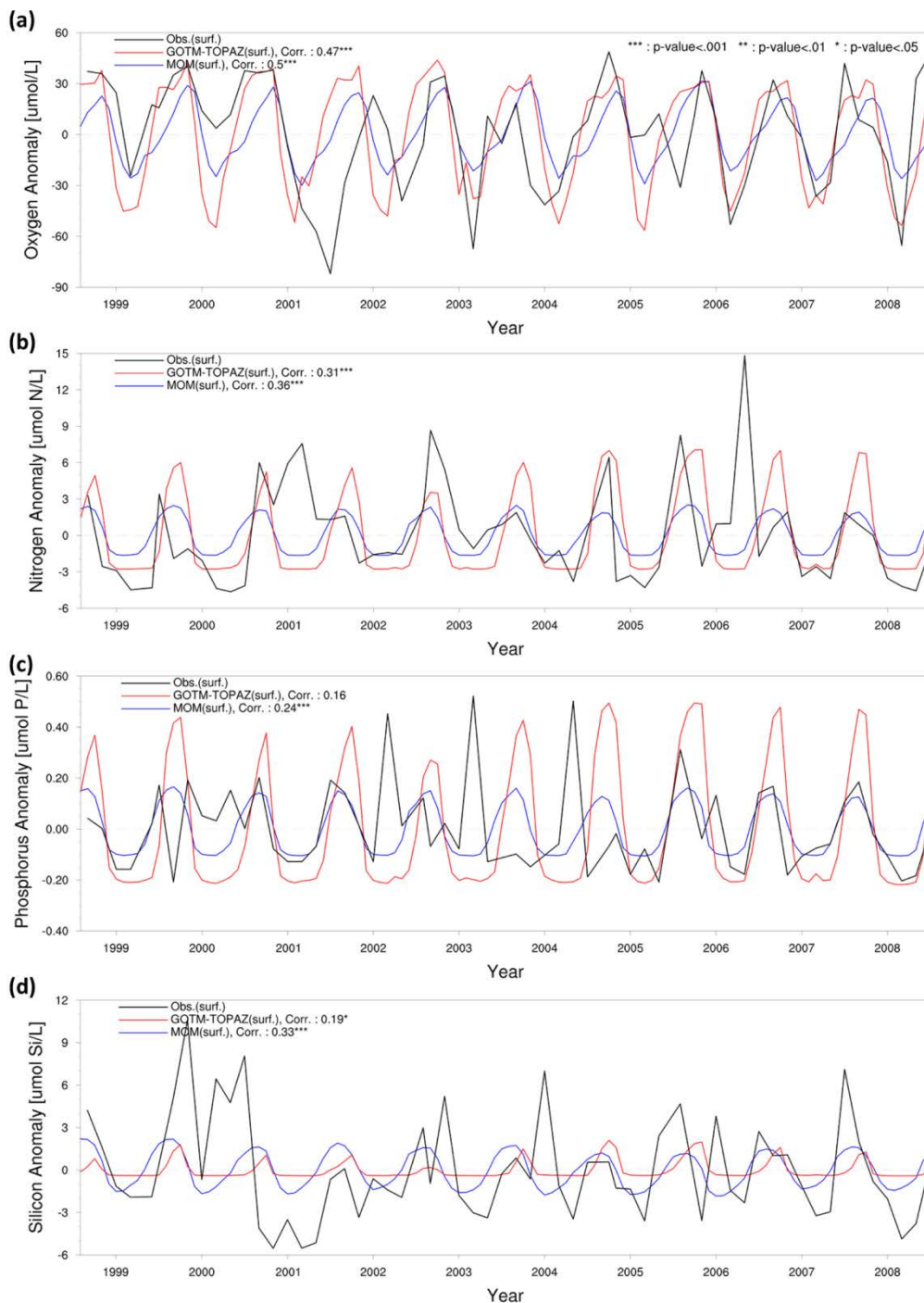
600

601



602

603 **Figure 4: Chlorophyll anomaly time series and correlation values for observational data (black lines), MOM5\_SIS\_TOPAZ results**  
 604 **(blue lines), and GOTM-TOPAZ results (red lines) for the 10-year period 1999–2008. (a), (c), and (e) are the mean values at depths**  
 605  **$\geq 20$  m and the correlations between the observations and each model at points 107, 104, and 102, respectively. (b), (d), and (f) are**  
 606 **the mean values at depths of 20–80 m and the correlation between the two models at points 107, 104, and 102, respectively.**



607

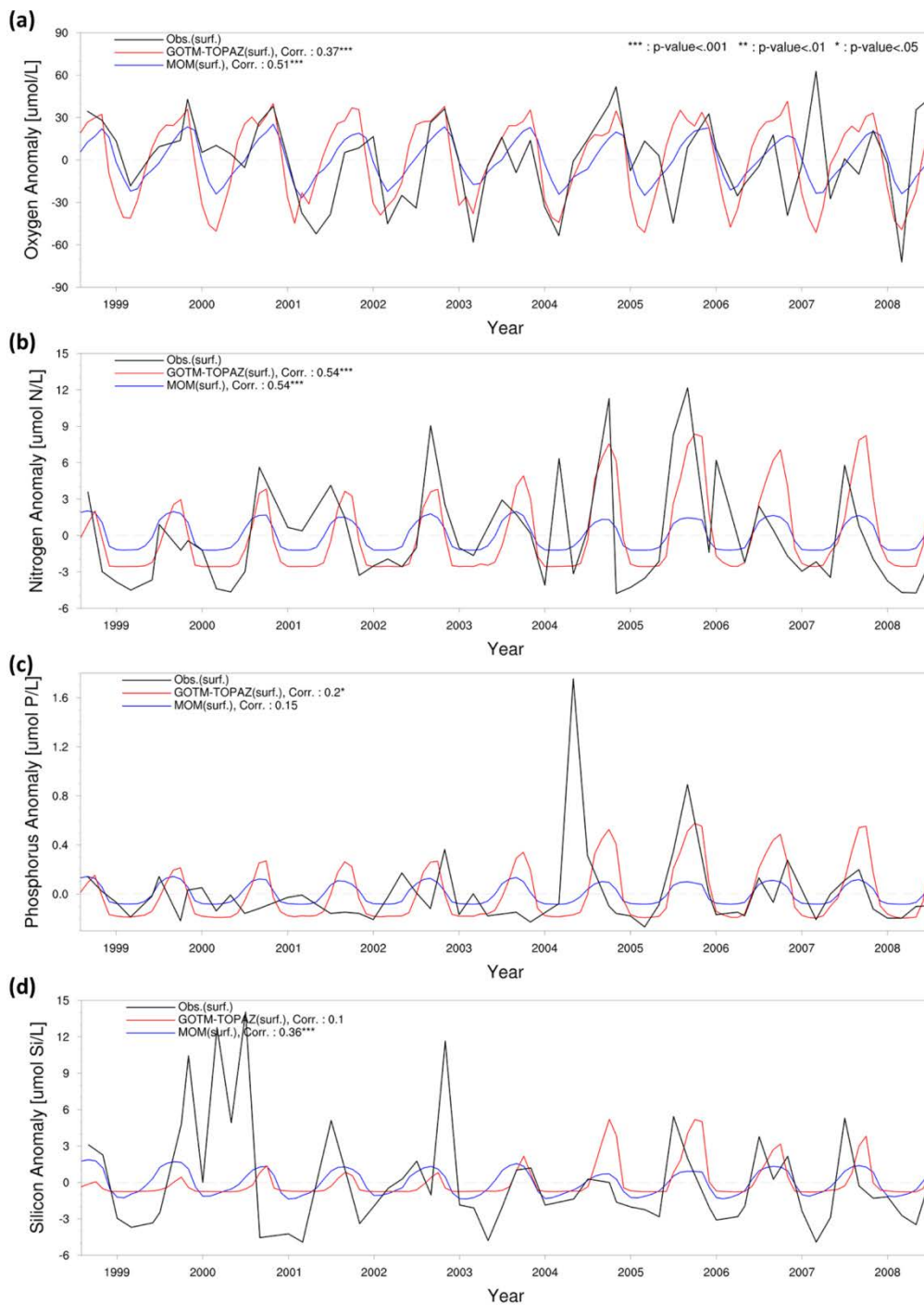
608

609

610

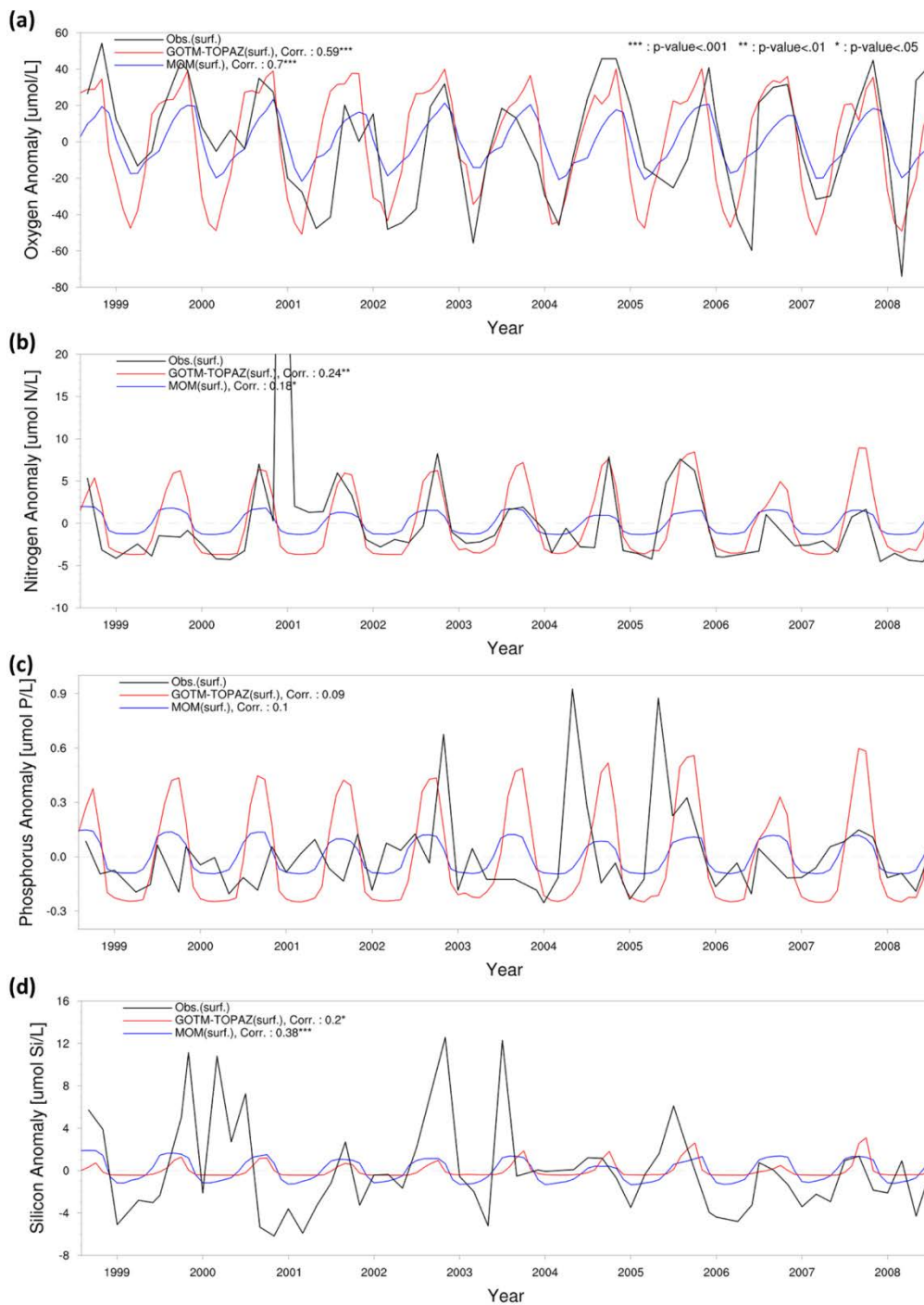
**Figure 5: Anomaly time series and correlation values from observational data (black lines), MOM results (blue lines), and GOTM-TOPAZ results (red lines) for concentrations of (a) dissolved oxygen, (b) nitrogen, (c) phosphorus, and (d) silicon at point 107 for the 10-year period 1999–2008; in this figure, nitrogen, phosphorus, and silicon include  $\text{NO}_3$ ,  $\text{PO}_4$ , and  $\text{SiO}_4$ , respectively.**





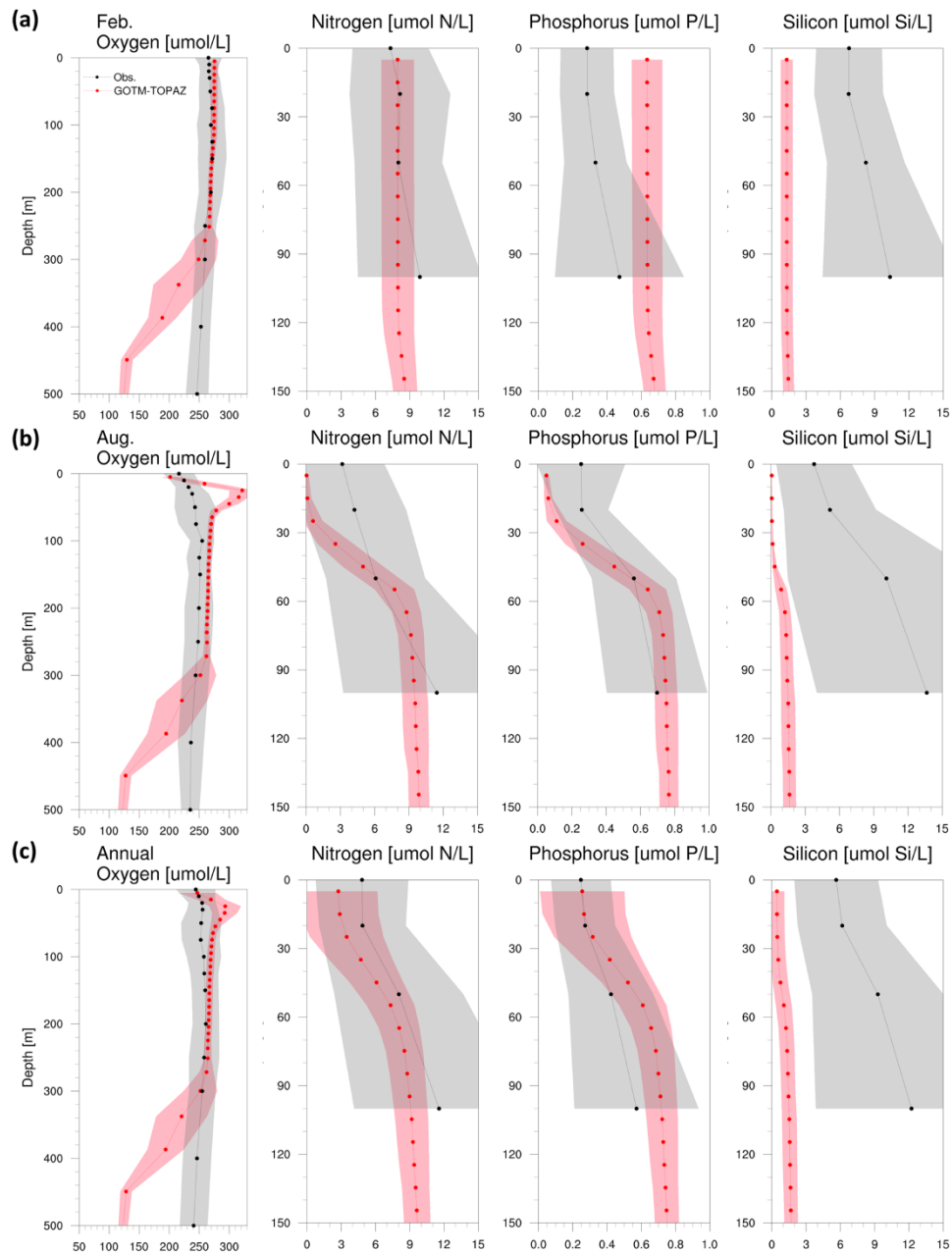
611

612 **Figure 6: Anomaly time series and correlation values from observational data (black lines), MOM results (blue lines), and GOTM-**  
 613 **TOPAZ results (red lines) for concentrations of (a) dissolved oxygen, (b) nitrogen, (c) phosphorus, and (d) silicon at point 104 for**  
 614 **the 10-year period 1999–2008; in this figure, nitrogen, phosphorus, and silicon include  $\text{NO}_3$ ,  $\text{PO}_4$ , and  $\text{SiO}_4$ , respectively.**



615

616 **Figure 7: Anomaly time series and correlation values from observational data (black lines), MOM results (blue lines), and GOTM-**  
 617 **TOPAZ results (red lines) for concentrations of (a) dissolved oxygen, (b) nitrogen, (c) phosphorus, and (d) silicon at point 102 for**  
 618 **the 10-year period 1999–2008; in this figure, nitrogen, phosphorus, and silicon include  $\text{NO}_3$ ,  $\text{PO}_4$ , and  $\text{SiO}_4$ , respectively.**

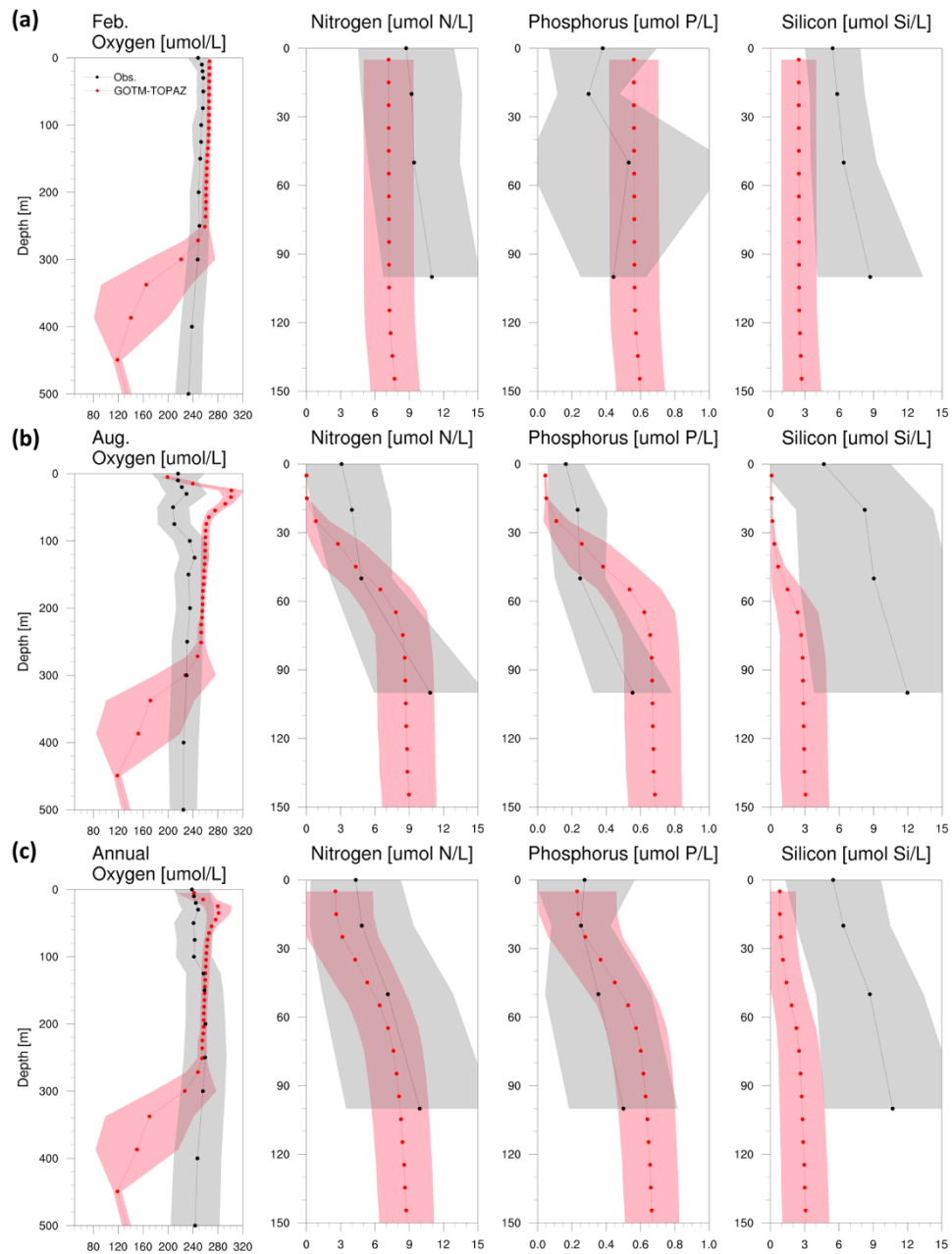


620

621 **Figure 8: Vertical profiles from observational data (black dots) and GOTM-TOPAZ results (red dots) at point 107 for**  
 622 **concentrations of dissolved oxygen, nitrogen, phosphorus, and silicon averaged from 1999–2008; (a) for February; (b) for August;**  
 623 **and (c) annually. The shaded areas represent 1 sigma. In this figure, nitrogen, phosphorus, and silicon include NO<sub>3</sub>, PO<sub>4</sub>, and SiO<sub>4</sub>,**  
 624 **respectively.**

625

626

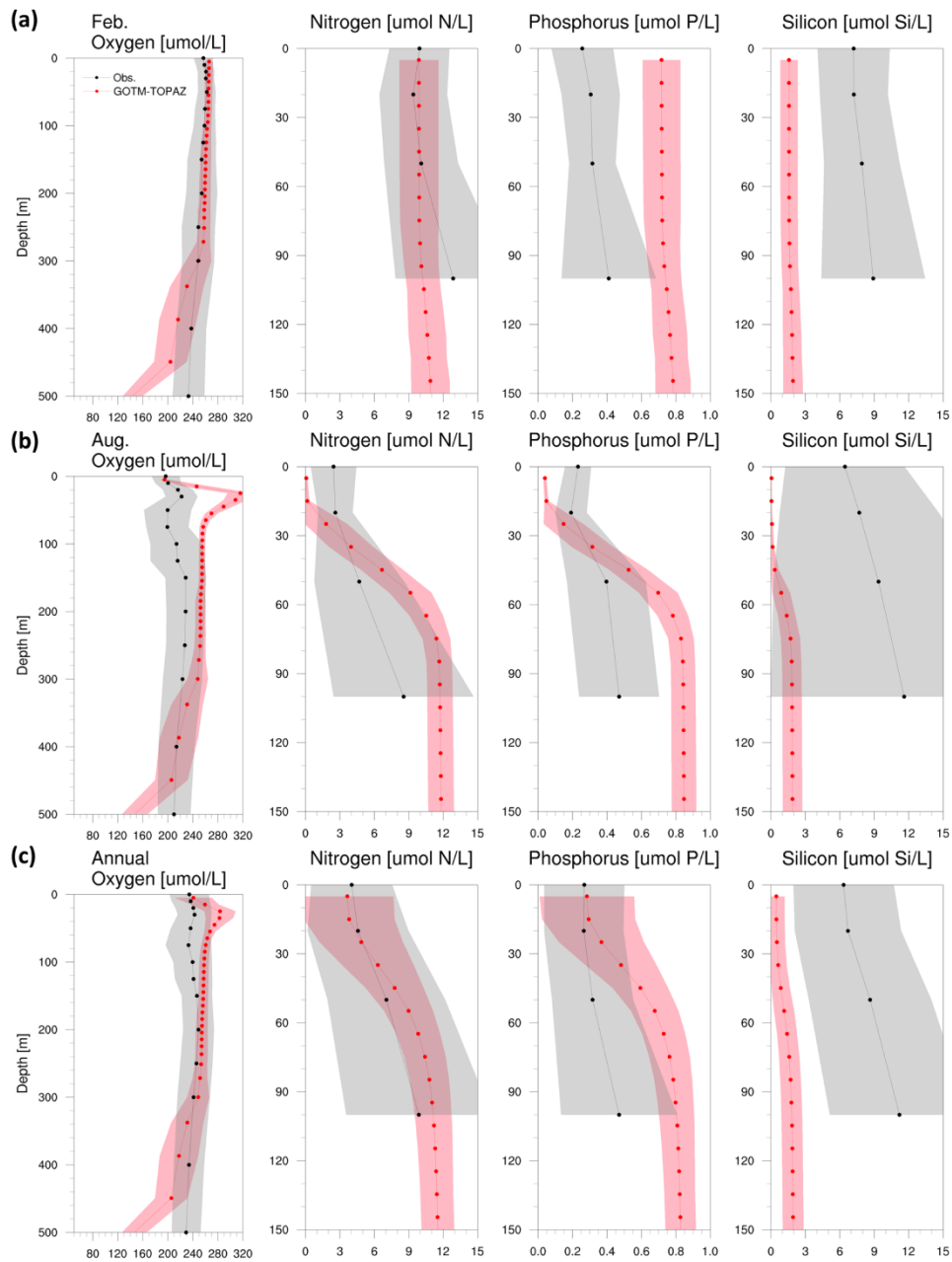


628

629 **Figure 9: Vertical profiles from observational data (black dots) and GOTM-TOPAZ results (red dots) at point 104 for**  
 630 **concentrations of dissolved oxygen, nitrogen, phosphorus, and silicon averaged from 1999–2008; (a) for February; (b) for August;**  
 631 **and (c) annually. The shaded areas represent 1 sigma. In this figure, nitrogen, phosphorus, and silicon include  $\text{NO}_3$ ,  $\text{PO}_4$ , and  $\text{SiO}_4$ ,**  
 632 **respectively.**

633

634

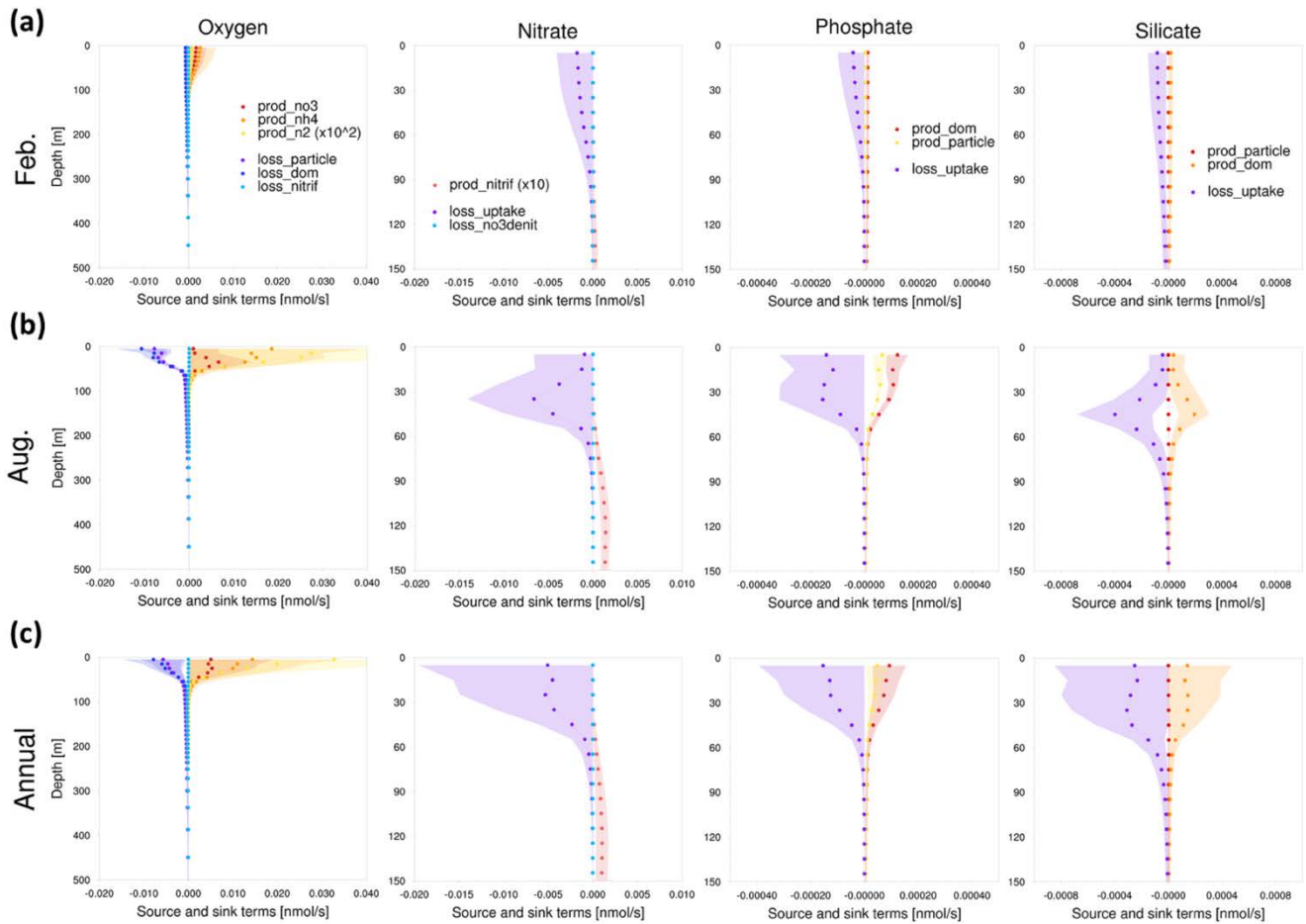


636

637 **Figure 10: Vertical profiles from observational data (black dots) and GOTM-TOPAZ results (red dots) at point 102 for**  
 638 **concentrations of dissolved oxygen, nitrogen, phosphorus, and silicon averaged from 1999–2008; (a) for February; (b) for August;**  
 639 **and (c) annually. The shaded areas represent 1 sigma. In this figure, nitrogen, phosphorus, and silicon include  $\text{NO}_3$ ,  $\text{PO}_4$ , and  $\text{SiO}_4$ ,**  
 640 **respectively.**

641

642



644

645 **Figure 11: Vertical profiles of the tendencies of source and sink terms in GOTM-TOPAZ at point 107 for the 10-year period 1999–**  
 646 **2008; (a) for February; (b) for August; and (c) annually. The shaded areas represent 1 sigma.**

647

648

649

650

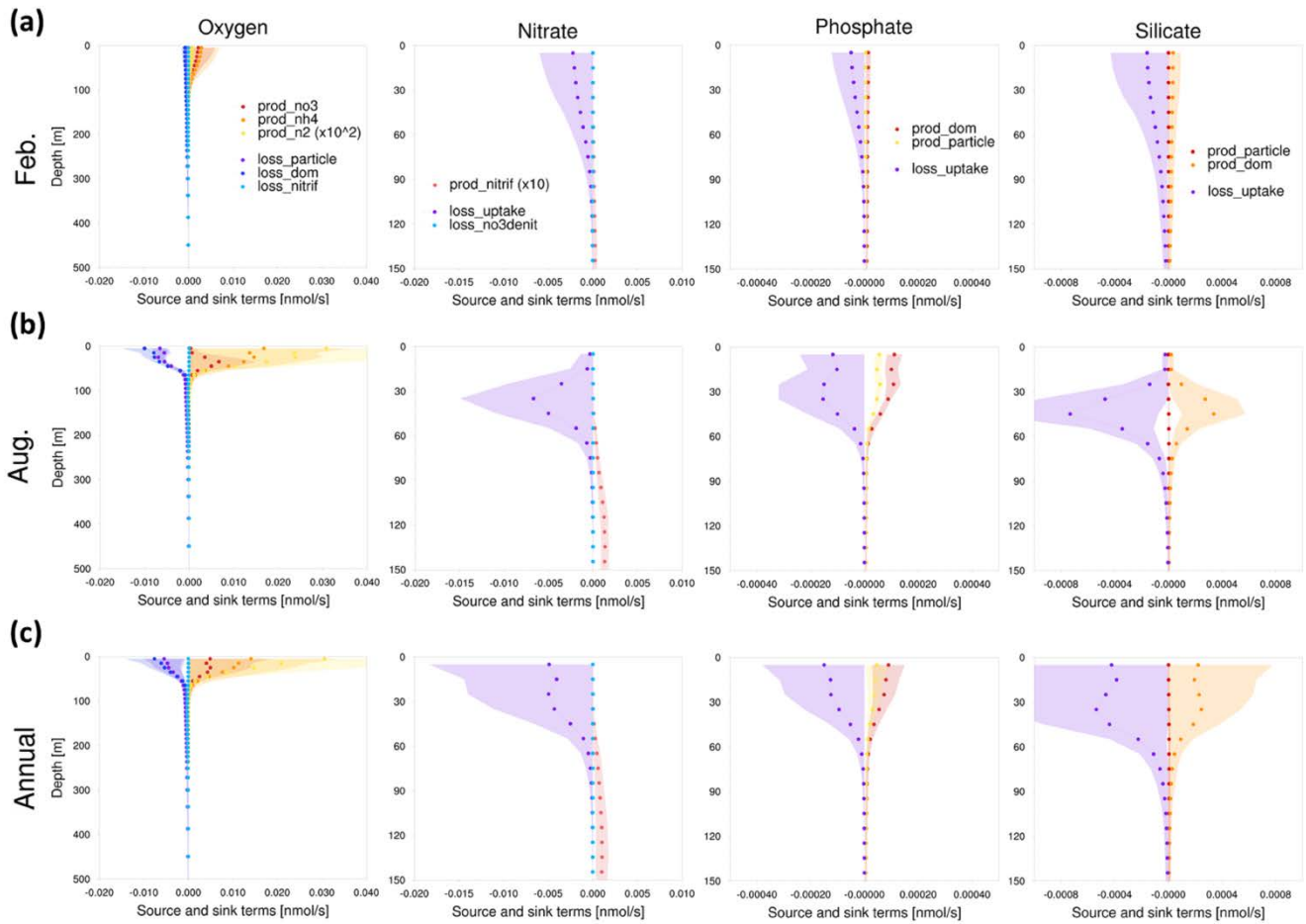
651

652

653

654

655



657

658 **Figure 12: Vertical profiles of the tendencies of source and sink terms in GOTM-TOPAZ at point 104 for the 10-year period 1999–**  
 659 **2008; (a) for February; (b) for August; and (c) annually. The shaded areas represent 1 sigma.**

660

661

662

663

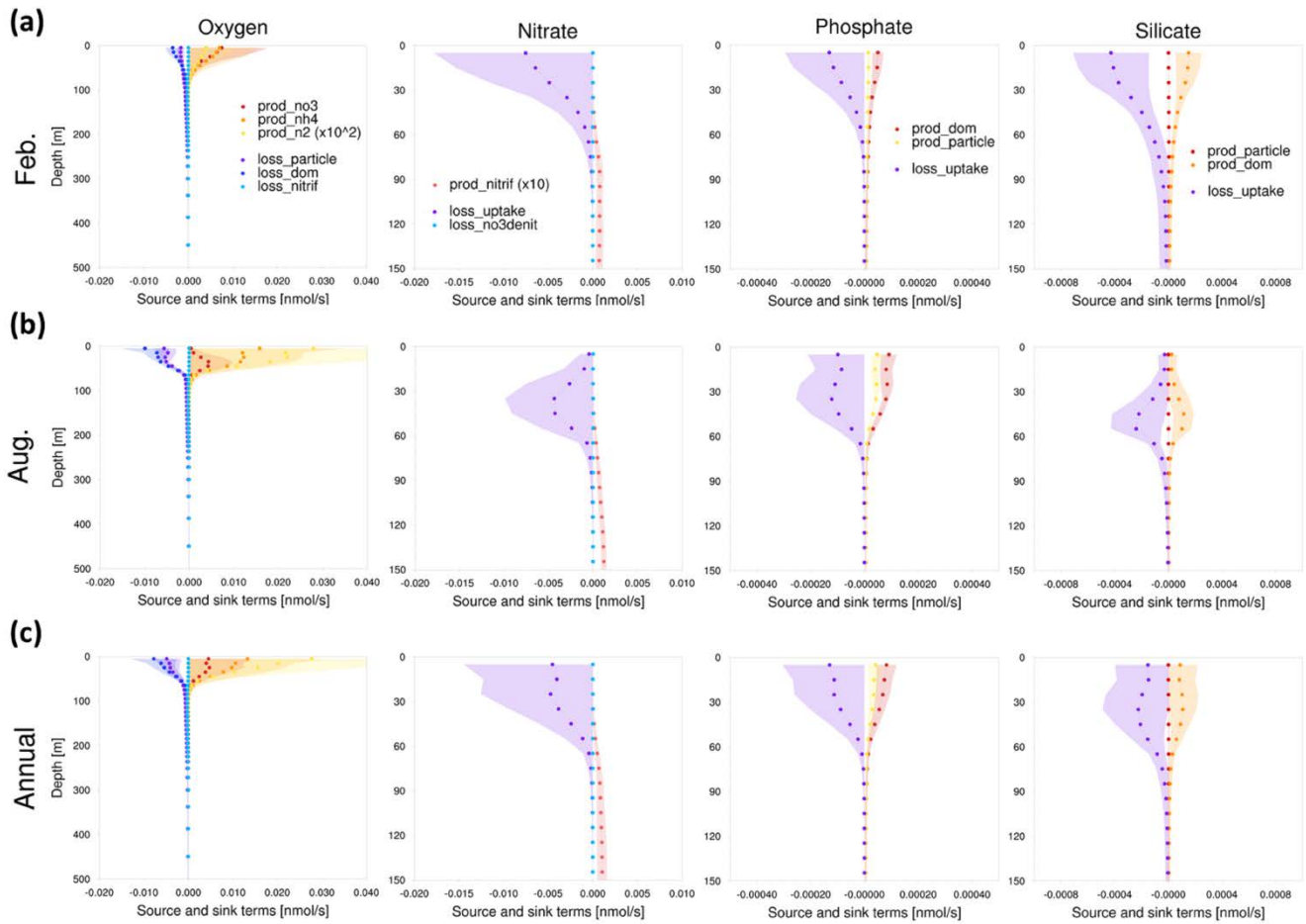
664

665

666

667

668



670

671 **Figure 13: Vertical profiles of the tendencies of source and sink terms in GOTM-TOPAZ at point 102 for the 10-year period 1999–**  
 672 **2008; (a) for February; (b) for August; and (c) annually. The shaded areas represent 1 sigma.**

673

674

675

676

677

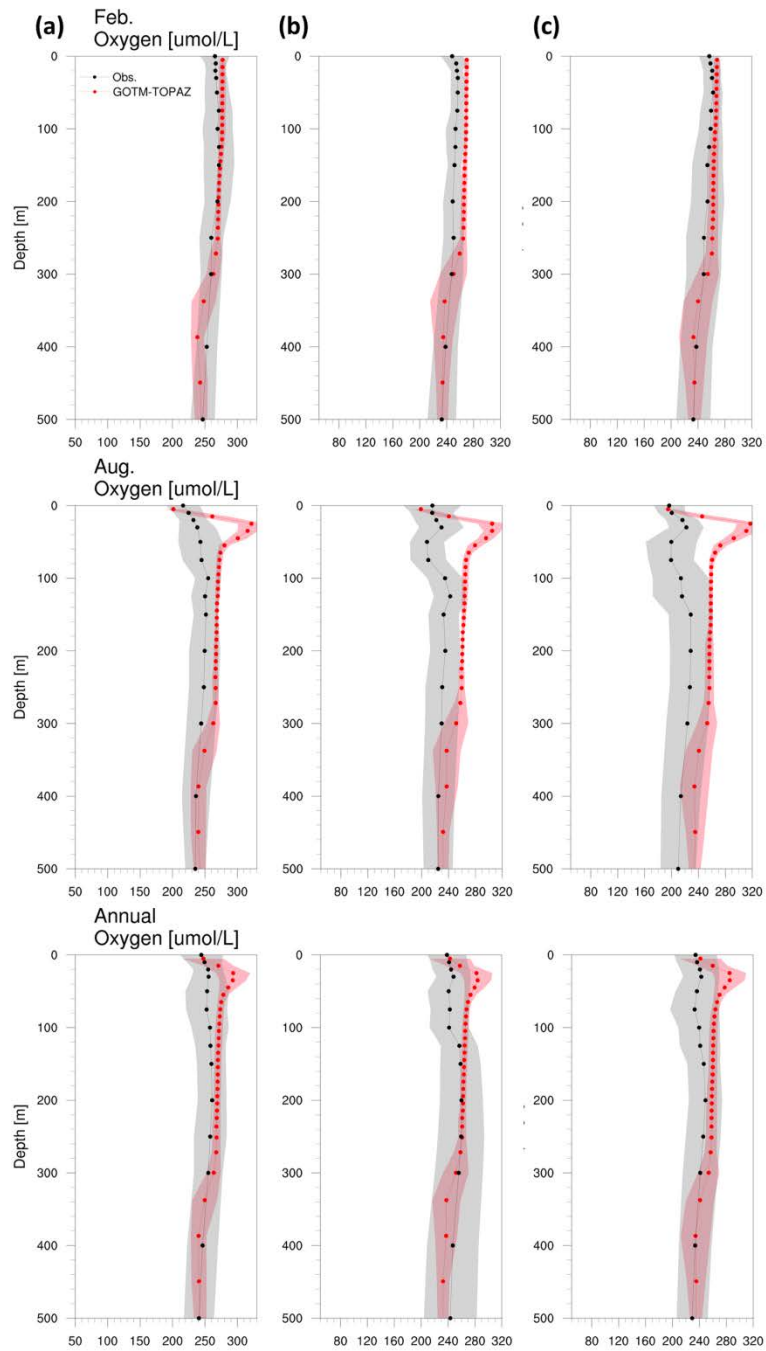
678

679

680

681

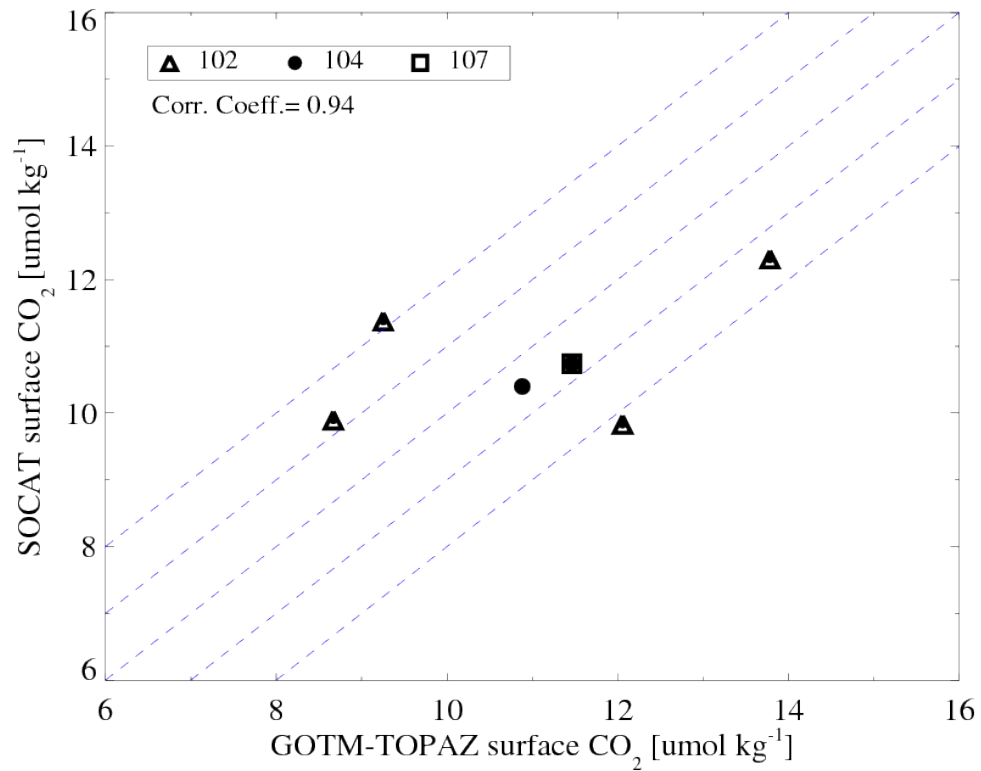




683

684 **Figure 14: Vertical profiles from observations (black dots) and GOTM-TOPAZ results (red dots) for concentrations of dissolved**  
 685 **oxygen averaged from 1999–2008; (a) for point 107; (b) for point 104; and (c) for point 102. GOTM-TOPAZ is simulated by**  
 686 **prescribing observations for the initial data. The shaded areas represent 1 sigma.**

687



689

690 **Figure 15: Scatterplot of mean monthly sea surface CO<sub>2</sub> concentrations as observed by the Surface Ocean CO<sub>2</sub> Atlas and**  
 691 **simulated by GOTM-TOPAZ. The thin dotted lines around the 1-to-1 line represent ±1 and 2 μmol kg<sup>-1</sup>.**

692

<b>Abbreviation</b>	<b>Full form</b>
<b>ESM</b>	Earth System Model
<b>SCM</b>	Single Column Model
<b>OGCM</b>	Ocean Global Circulation Models
<b>CMIP5</b>	Coupled Model Intercomparison Project 5 (fifth phase)
<b>GFDL</b>	Geophysical Fluid Dynamics Laboratory
<b>ARCCSS</b>	Australian Research Council Centre of Excellence for Climate System Science
<b>NIFS</b>	National Institute of Fisheries Science
<b>ESM2M</b>	Earth System Model version 2, with Modular Ocean Model Version 4.1
<b>ESM2G</b>	Earth System Model version 2, with General Ocean Layer Dynamics
<b>ECMWF</b>	European Centre for Medium-Range Weather Forecasts
<b>GOTM</b>	General Ocean Turbulence Model
<b>TOPAZ</b>	Tracers of Phytoplankton with Allometric Zooplankton
<b>MOM5</b>	Modular Ocean Model version 5
<b>NEMO</b>	Nucleus for European Modelling of the Ocean
<b>MEDUSA</b>	Model of Ecosystem Dynamics, Nutrients Utilization, Sequestration and Acidification
<b>PISCES</b>	Pelagic Interactions Scheme for Carbon and Ecosystem Studies
<b>SOCAT</b>	Surface Ocean CO <sub>2</sub> Atlas
<b>SeaWiFS</b>	Sea-viewing Wide Field-of-view Sensor
<b>CORE-II</b>	Coordinated Ocean-ice Reference Experiments II
<b>PAR</b>	Photosynthetically Active Radiation
<b>TWC</b>	Tsushima Warm Current
<b>EKWC</b>	East Korea Warm Current
<b>NKCC</b>	North Korea Cold Current
<b>NB</b>	Nearshore Branch
<b>OB</b>	Offshore Branch
<b>ESIW</b>	East Sea Intermediate Water